NASA-TM-106660 19960001336

NASA Technical Memorandum 106660

TROPIX Power System Architecture

David B. Manner
Sverdrup Technology, Inc.
Ames Research Center
Moffett Field, California

and

J. Mark Hickman
Lewis Research Center
Cleveland, Ohio

LIBRARY COPY

OCT 1 1995

LANGLEY RESEARCH CENTER
LIBRARY, NASA
HAMPTON, VIRGINIA

September 1995

National Aeronautics and
Space Administration

NASA Technical Library
3 1176 01423 0065

Contents

List of Tables

List of Figures

Chapter 1

Introduction

This document contains results obtained in the process of performing a power system definition study of the TROPIX power management and distribution system (PMAD). Requirements derived from the PMADs interaction with other spacecraft systems are discussed first. Since the design is dependent on the performance of the photovoltaics, there is a comprehensive discussion of the appropriate models for cells and arrays. A trade study of the array operating voltage and its effect on array bus mass is also presented. A system architecture is developed which makes use of a combination of high efficiency switching power convertors and analog regulators. Mass and volume estimates are presented for all subsystems.

A FORTRAN program was developed to determine the peak power point of a photovoltaic cell, given cell parameters. This program was developed using Microsoft Fortran 5.0. Numerous spreadsheet workfiles were developed to produce tables and figures using Lotus 123 Revision 3.0. Schematics were developed using OrCad SDT.

As a result of the spacecraft's rather long exposure to the plasma in low earth orbit, early efforts attempted to devise a method which would mitigate the undesirable effects which result. Low voltage (28V) negative ground arrays were one possible solution. This solution pays a mass penalty in the form of increased weight of the photovoltaic array bus wiring. A unique architecture

was discovered, using a buck/boost convertor for primary power conversion. Using a reverse polarity buck/boost convertor, the arrays can be positively grounded while the loads remain negatively grounded.

This concept enables the power system designer to operate the photovoltaic arrays at high voltages with greatly reduced risk of arcing and sputtering. A scientific paper describing this concept in the context of the low earth orbit plasma was composed by Manner, Herr and Ferguson, and should be appearing in a technical journal soon. Prepublication copies are available from the author. The unique nature of this discovery, and the potential usefulness to all spacecraft transiting the low earth orbit plasma have motivated a patent application.

I would like to express my thanks to Mark Hickman (NASA LeRC) and John Bozek (NASA LeRC) for their support and enthusiasm throughout this project.

DBM

Chapter 2

Requirements

The requirements detailed in this section include those needed to determine the power management and capacity. This is largely based on load requirements in the form of voltage and power demand. Also included are requirements connected with other systems that effect the PMAD design. These include battery capacity and charging requirements, and various operating environment considerations.

TROPIX is required to operate in an high inclination, slow outward spiral trajectory, starting in low earth orbit and terminating at geosynchronous orbit altitude. Thermal and plasma effects are quite different as the mission progresses, and have a significant impact on the power system architecture.

The distributed electric field on the photovoltaic arrays affects the electron and ion currents exchanged with the plasma. The tendency of the spacecraft immersed in the LEO plasma, is to accumulate a net negative charge. This tends to drive the array negative terminal to a negative voltage and the positive terminal to a slightly positive voltage with respect to the plasma potential. For typical spacecraft configurations, the positive terminal floats above the plasma potential by about 10% of the operating voltage, and the negative terminal floats about 90% below.

If the spacecraft hull is grounded in the conventional way, to the negative array terminal, the hull potential will be negative with respect to the plasma. This presents no problem if the array operating voltage is a standard 28 volts,

resulting in a hull potential of about -25 V. Choosing to operate the arrays at a higher voltage will drive this potential more negative. There is a threshold at approximately -40 V at which electrostatic discharges and sputtering of spacecraft surfaces becomes a threat. This constraint would limit negative ground power systems to a maximum photovoltaic array operating voltage to about 45 volts.

Positive grounding provides many benefits by minimizing interactions with the plasma. Of particular importance is the small potential difference between the positive grounded hull and the plasma potential. The 160 volt arrays planned for Space Station Freedom, if positive grounded, would hold the hull potential at about +16 V, a sufficiently small potential to be of little concern. The distributed electric field on the panels will actively drive the hull potential. The plasma contactor hardware could be eliminated entirely since this function is performed by the arrays themselves. Positive grounding is not without cost, however.

Positive grounding does complicate the power conversion, distribution, load grounding. This is due to two principle problems. First, most electronic equipment is designed and built to be used in a negative ground architecture. This difficulty can be handled in several ways, all with mass and complexity penalties. Second, the availability of P-channel and PNP semiconductors is rather limited. This difficulty can be handled by carefully selecting from available components, and with alternative designs which use N-channel and NPN semiconductors.

Since there are considerable wiring mass savings associated with high voltage arrays, an acceptable positive ground architecture was sought.

2.1 Load Requirements

Demand for electrical power originates with the following loads: 1) science payloads, 2) guidance, navigation and control, 3) command and data handling, 4) communications, and 5) propulsion systems. Table 2.1 lists the power requirements for each.

	Qty	Sun Total Demand (W)	Shade Total Demand (W)	Load Volt (V)	Load Reg (V)
Science Payloads					
Langmuir Probe	1	1.0	1.0	28.0	± 2.0
V-Body Probe	1	1.0	1.0	28.0	± 2.0
Signal Conditioner	1	2.0	2.0	28.0	± 2.0
Pressure Gauge	1	2.0	2.0	28.0	± 2.0
Exp. - CPU	1	19.0	19.0	28.0	± 2.0
Exp. - A/D	2	24.0	24.0	28.0	± 2.0
Exp. - memory	2	24.0	24.0	28.0	± 2.0
Exp. - fast A/D	1	5.5	5.5	28.0	± 2.0
Exp. - I/O	1	5.5	5.5	28.0	± 2.0
Exp. - relays	1	1.0	1.0	28.0	± 2.0
Exp. - Electrometer	1	65.0	0.0	28.0	± 2.0
Exp. - Power Supply	1	19.0	19.0	28.0	± 2.0
Exp. - Power Supply	1	10.0	10.0	28.0	± 2.0
M/E Particle Detector	2	40.0	40.0	28.0	± 2.0
H/E Particle Detector	1	5.0	5.0	28.0	± 2.0
Command and Data Handling					
Main Computer	1	*.*	*.*	28.0	± 2.0
Telemetry and Command	1	10.0	10.0	28.0	± 2.0
Communications					
Transmitter	1	31.5	31.5	28.0	± 7.0
Receiver	1	4.5	4.5	28.0	± 7.0
Thermal					
Payload thermal supp.	1	1.0	1.0	28.0	± 2.0
Mechanisms					
Array positioning	2	30.0	2.0	28.0	± 2.0
GN&C					
GPS receiver	1	3.5	3.5	28.0	± 12.0
Inertial Unit	1	10.4	10.4	28.0	± 2.0
Sun sensor	2	1.0	0.0	28.0	± 2.0
ERADS	1	23.0	23.0	28.0	± 2.0
Shade Systems					
Batteries	1	***.0	*.*	80.0	±20.0
Charge regulator	1	***.0	*.*	80.0	±20.0
Discharge regulator	1	***.0	*.*	80.0	±20.0
Primary Propulsion					
Thrusters	2	1749.0	0.0	80.0	±20.0
Gimbals	1	8.3	0.0	28.0	± 5.0

Table 2.1: Electrical Load Requirements

2.2 Battery Functions

The Battery Requirements Document provides a detailed analysis of the required battery capacity, voltage, and technology to be used by the TROPIX spacecraft. Battery requirements are considered here only to the extent that they affect the charge and discharge electronics.

The battery supplies power to the spacecraft during periods of eclipse. It is also used for peaking, when energy demand exceeds production. Required capacity is determined from the eclipse period in which there is the largest demand for energy. Charging will take place when excess power is available from the photovoltaic arrays. For instance, when the spacecraft first emerges from eclipse and the photovoltaic arrays are cold, their output power is considerably higher than normal. This excess power is captured by charging the battery rapidly.

The electric thrusters will only be operated when the spacecraft is out of eclipse. The TROPIX power system architecture is designed so that energy is delivered directly to the thruster's power processing unit from the photovoltaic array. No energy storage is required for thruster operations.

The number of charge and discharge cycles that a battery can tolerate before its performance is degraded depends on numerous factors, including overcharging, and deep cycling. Overcharging can be the result of excessive current flow causing overheating or, a float voltage used to keep the batteries "topped up" which too high. Deep cycling refers to charge and discharge cycles in which the battery is allowed to completely (or almost completely) discharge. The battery charge electronics are required to prevent overcharging and maintain the batteries at full charge when excess energy is available. The battery capacity is determined largely based upon cycle depth considerations.

2.3 Battery Requirements

Power is supplied by the battery when the demand for power from the loads exceeds the power available. Similarly, power is supplied to the battery for

total capacity	440	W-hr
discharge time	35 - 70	min
charge time	60 - 1500	min
charge/discharge	932	cycles
discharge rate	307	W maximum
charge rate	256	W maximum
discharge energy	351	W-hr minimum
depth of discharge	80	% maximum
operational life	1	year
nominal voltage	28	volts
operating temperature	27	C
minimum temperature	-18	C
maximum temperature	52	C

Table 2.2: Battery Performance Requirements

charging when available power exceeds demand. At any point during the mission, the state of charge of the battery can be computed by integrating the difference between available power and power demand over time, and accounting for losses in the charge and discharge electronics. An detailed analysis of the power flowing to and from the battery, and state of charge over the life of the mission is available in the Battery Requirements Document.

Deep cycling a battery tends to reduce its useful life. Charge and discharge cycling, and the required battery life are used to determine a minimum allowable state of charge. Once this minimum has been set, the battery capacity can be found. For the baseline TROPIX mission, the minimum state of charge takes place during (TBD) mission phase. Assuming the minimum state of charge is 20%, a battery capacity of 440 W-hrs was determined.

TROPIX will use nickel-cadmium (NiCd) batteries. Flight qualified batteries are available and the charge and discharge requirements to maintain long life are well understood. Table 2.2 includes a synopsis of the battery performance requirements.

	State of Charge	volts/cell	output voltage
full	100%	1.25	30.0
nominal	80% - 40%	1.15	27.6
max depth	20%	1.00	24.0

Table 2.3: Battery Cell and Output Voltages

The NiCad cell voltages during discharge appear in Table 2.3. Using a nominal cell voltage of 1.15 volts per cell implies that the battery is composed of 24 cells in series with maximum and minimum voltages also appearing in Table 2.3. The minimum state of charge allowed is 20%.

2.3.1 Battery Charger Requirements

The battery charger electronics are required to charge the battery quickly when excess energy is available, and prevent overcharging. When the battery is fully charged and excess power is available, the charger is required to reject power in excess of that required to maintain the battery at full charge with the appropriate float voltage.

The battery charger will initially charge at the highest possible rate while protecting against overheating or reduction in the charge/discharge life below 932 cycles by limiting current. For a battery capacity of C_{batt} (W-hr), this energy flow limit was selected to be 58% of the capacity or

$$P_{\text{max}} = C_{\text{batt}}/1.72$$

Full charge is indicated when the battery terminal voltage reaches the full charge threshold voltage. The charger will then switch to a voltage float mode which will maintain a constant voltage across the battery terminals and provide a trickle current sufficient to keep the battery in a fully charged state without overcharging. Table 2.4 contains the pertinent values.

Maximum initial charge rate	256	Watts
Maximum initial charge current	9	Amps
Full charge threshold voltage	1.33	Volts/Cell
	31.9	Volts
Trickle charge float voltage	1.25	Volts/Cell
	30.0	Volts

Table 2.4: Battery Charger Requirements

2.3.2 Battery Discharging

The battery discharge electronics are required to boost the 28 volt nominal battery output into a 32 volt minimum supply for the load voltage regulator.

The discharge electronics will provide a high efficiency (92%) drive with good regulation (34 $\pm$ 2 V) over the entire range of battery discharge voltages.

The maximum demand from the loads during battery discharge cycles is 307 W at 28 volts or about 11 amps.

2.4 Photovoltaic Arrays

The TROPIX photovoltaic array consists of of two wings mounted on a gimbal shaft, and one extending left and one extending right of the spacecraft. Wing areas are $6.13m^2$, for a total photovoltaic array area of $12.26m^2$. Using gallium arsenide cells and assuming 18.5% efficiency, each wing produces 1.1 KW, based on 1368 W/m^2 at AM0 (atmosphere zero) available in the form of solar insolation. Cells are assumed to be standard 4 cm$\times$4 cm profile. The internal wiring of the array connects individual cells, using a series and parallel arrangement in order to develop appropriate operating voltages and supply currents.

2.5 Operating Environment

The space environment which TROPIX must withstand changes considerably as the as the spacecraft spirals out from a low earth orbit (LEO) at 325km to geosynchronous (GEO) orbit altitudes of 35900km. The plasma density, plasma energy, temperatures and spacecraft charging effects are all quite different in these two regimes.

2.5.1 Thermal

Arrays will be required to withstand and operate at temperatures of -80C to +80C. Temperatures inside the spacecraft will be assumed to be within the standard military electronics range of -55C to 100C. Nominal operating temperature is assumed to be 42C.

2.5.2 Altitude

As the as the spacecraft spirals out from a low earth orbit at 325km to a geosynchronous orbit at 35900km, the plasma density, plasma energy, temperatures and vary considerably. Since plasma interactions can have a dramatic effect on spacecraft charging, a power system architecture which minimizes these effects is desirable.

2.5.2.1 LEO

Low earth orbit is characterized by the relatively dense plasma which exists there. It is four to six orders of magnitude more dense than plasma which exists in GEO. Temperatures are relatively low and the resulting plasma energies are on the order of 0.1 eV.

Since electron mass is much less than ion masses, the average velocities for plasma electrons are much higher than those of ions. This effect causes the spacecraft to accumulate a net negative charge. The result of this charge separation is an electric field which attracts positive ions. The floating potential of the spacecraft hull continues to decrease until the electron and ion currents are in balance. At equilibrium, these currents are on the order of milliamps per square meter.

Dielectric surfaces exposed to the LEO plasma typically float to a voltage which is a few volts negative with respect to plasma potential.

Dielectric backing of the PVA is favored in LEO.

2.5.2.2 GEO

The plasma associated with geosynchronous orbits is characterized by a low density plasma. Temperatures are much higher than LEO and the resulting plasma energies are on the order of 1000 eV.

During quiescent periods, a low current flux is typical, on the order of microamps per square meter, resulting in little spacecraft charging. However, during a geomagnetic storm the high energy of the plasma can produce a large negative floating potential on the hull of the spacecraft. A floating potential of -1 to -2 kV is possible. Differential charging of spacecraft surfaces can lead to sufficiently high potentials that electrostatic discharges become a concern.

Conductive grounded backing is favored in GEO since it distributes accumulated charge rapidly and will hold the back surface of the PVA near hull potential.

Chapter 3

Photovoltaic Models

Considerable effort was directed toward developing accurate models for the photovoltaic cells, arrays and configuration. gallium arsenide on germanium was the selected material. This was based on several factors:

1. GaAs cells have a fairly high conversion efficiency (18.5%) compared to silicon cells.
2. Power available from the cells is derated by 0.24% per degree centigrade. This is much less than that for silicon.
3. Gallium arsenide arrays are lightweight.
4. Gallium arsenide cell are resistant to radiation damage.
5. Blocking diodes may not be required if select cells are used to construct the arrays.

3.1 GaAs cell model

The GaAs cell model used is ideal and conventional. It consists of an ideal diode model with an additional junction current source derived from impingement of light. Figure 3.1 shows the positive sign conventions for voltage and current, which correspond with the actual sense of each, when the

cell is producing power. This schematic was created using OrCad SDT. The light induced current is represented by J_λ, and the dark diode reverse bias current is represented by J_{rb}.

The constitutive equation for this idealized model is

$$J = J_\lambda - J_{rb}(e^{\frac{V}{V_{th}}} - 1) \tag{3.1}$$

where,

$$V_{th} = \frac{AkT}{q}$$

with diode constant, A; Boltzman's constant, $k = 1.38E-23$ (J/K); absolute temperature, T (K); electron charge, $q = 1.6E-19$ coulombs. Diode constant, A is generally in the range of 1-5 depending on material, junction depth, etc. GaAs solar cells typically have $A \approx 1$. Note that current has been normalized by dividing by the light collection area, so that

$$J = I/A_c$$

The open circuit voltage produced by an illuminated cell can be found by setting $J = 0$, $V = V_{oc}$ and solving Equation 3.1,

$$V_{oc} = V_{th} \ln \frac{J_{sc}}{J_{rb}} + 1$$

Similarly, the short circuit current produced by an illuminated cell can be related to the diode reverse bias current by setting $V = 0$, $J = J_{sc}$, and solving Equation 3.1, or

$$J_{sc} = J_\lambda = J_{rb}(e^{\frac{V_{oc}}{V_{th}}} - 1)$$

Since the open circuit voltage and short circuit current are usually specified by the manufacturer, an expression relating the device current and voltage can be expressed as

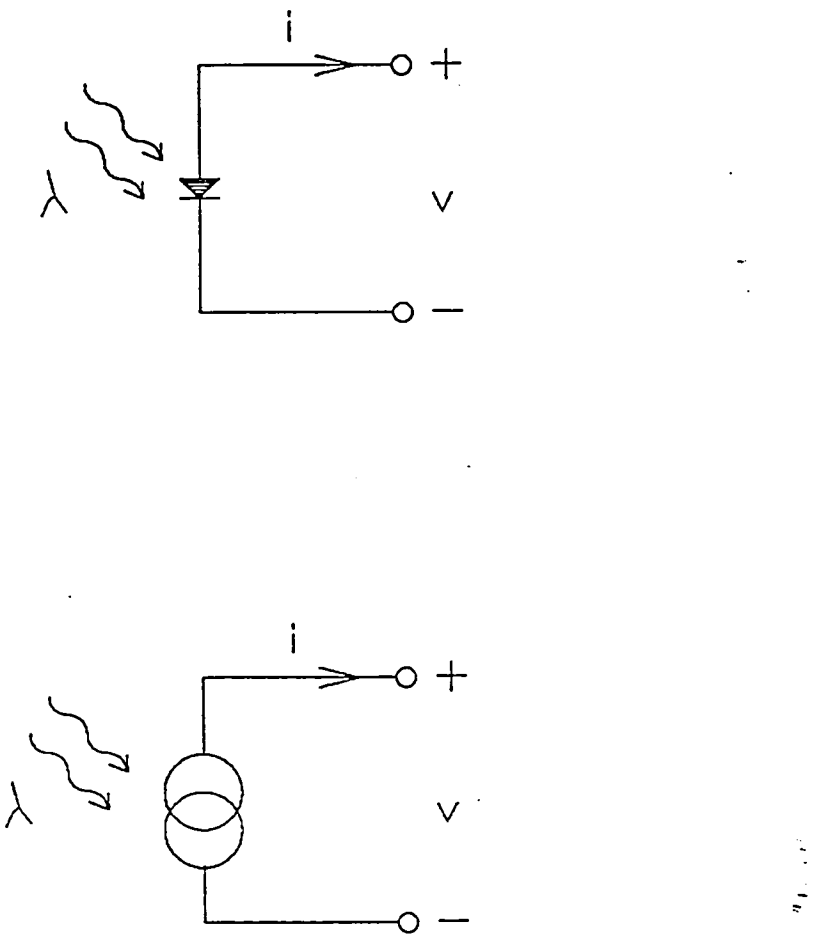

Figure 3.1: Photovoltaic Cell Schematic Representation

$$J = J_{sc}\frac{\left(e^{\frac{V_{oc}}{V_{th}}} - e^{\frac{V}{V_{th}}}\right)}{\left(e^{\frac{V_{oc}}{V_{th}}} - 1\right)} \tag{3.2}$$

This expression is equivalent to both the ideal JPL model and the Hughes model, assuming that the device series and shunt resistances are zero and infinite respectively. Figure 3.2 depicts the current versus voltage curve for a typical GaAs cell.

3.1.1 Photovoltaic Cell Power Output

The power output from a photovoltaic cell depends on the load presented. An expression for the output power can be formed by by multiplying Equation 3.2 by V,

$$P = VJ = VJ_{sc}\frac{\left(e^{\frac{V_{oc}}{V_{th}}} - e^{\frac{V}{V_{th}}}\right)}{\left(e^{\frac{V_{oc}}{V_{th}}} - 1\right)} \tag{3.3}$$

When this power is plotted versus output voltage, it tends to rise linearly for low voltages, peak and drop off rapidly as V_{oc} is approached. A plot of power versus output voltage appears in Figure 3.3. The maximum power output occurs at the point where a rectangle contained under the $J - V$ curve has the maximum area. This point, denoted P_{mp}, occurs at a voltage that is generally about 80% of V_{oc}.

A value for P_{mp} can be obtained by finding the value of V which makes the derivative of P with respect to V equal to zero. Rewriting the expression for P, let

$$P = Vk_1\left(k_2 - e^{\alpha V}\right)$$

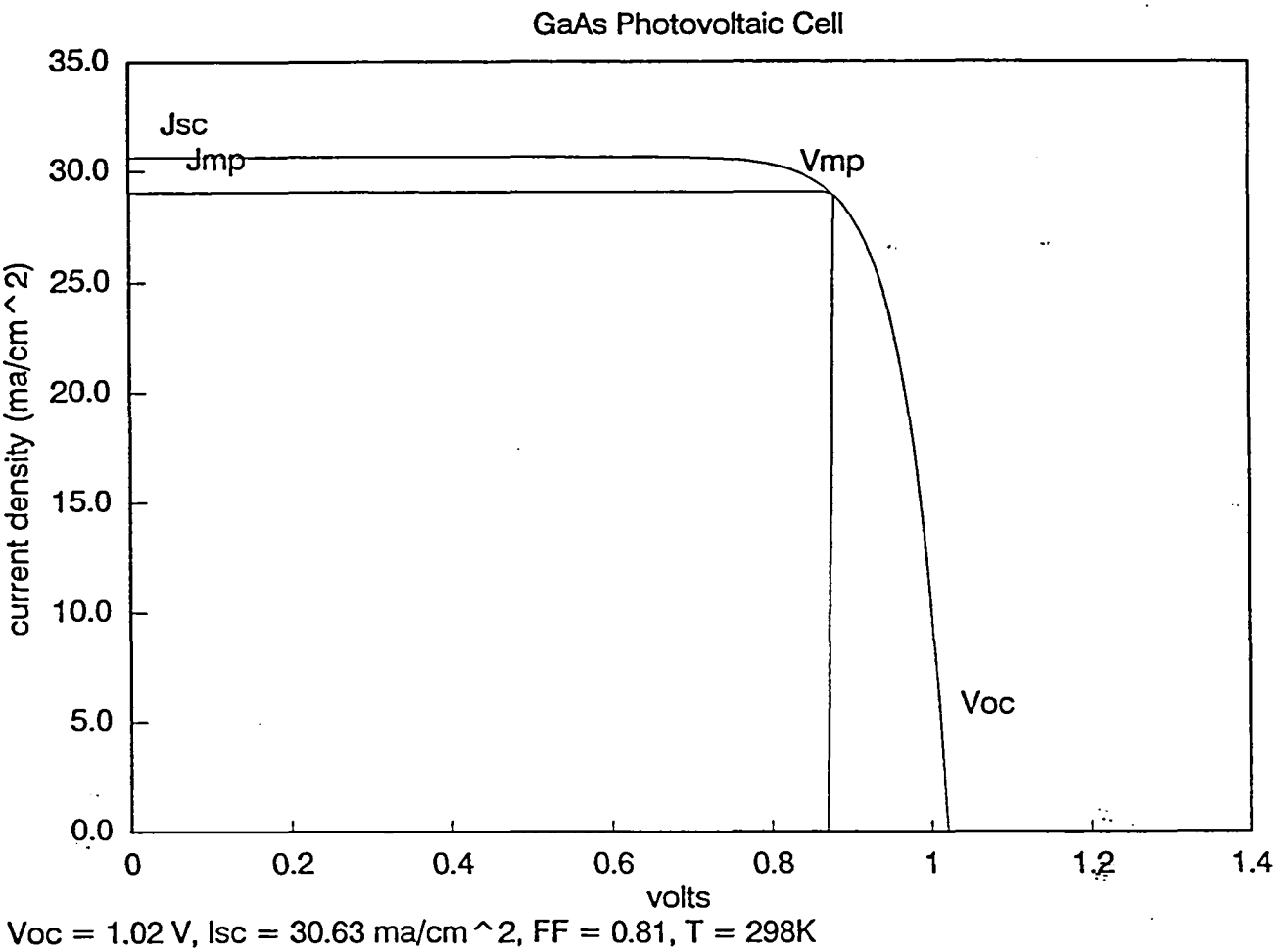

Figure 3.2: PVC J-V Characteristics

where

$$\alpha = \frac{1}{V_{th}} = \frac{q}{AkT}$$

$$k_1 = \frac{J_{sc}}{e^{\alpha V_{oc}} - 1}$$

$$k_2 = e^{\alpha V_{oc}}$$

Forming the partial derivative yields

$$\begin{aligned} \frac{\partial P}{\partial V} &= \frac{\partial}{\partial V}\left[k_1 k_2 V - k_1 V e^{\alpha V}\right] \\ &= k_1 k_2 - k_1\left[V\alpha e^{\alpha V} + e^{\alpha V}\right] \\ &= k_2 - e^{\alpha V}\left[1 + V\alpha\right] = 0 \end{aligned}$$

Eliminating constant k_2 and rearranging gives

$$e^{\alpha V_{oc}} = e^{\alpha V}\left[1 + V\alpha\right]$$

or,

$$1 + \alpha V - e^{-\alpha(V_{oc} - V)} = 0$$

Solving for V requires a method for searching over a range of voltages. The Newton-Raphson method will be use for this purpose and is discussed next.

The Newton-Raphson Method

The Newton-Raphson method is an iterative method for finding the zero crossing of a function, $f(V)$, when the derivatives, $f'(V)$, can be found. It can be used to find P_{mp} and converges quite rapidly using

$$V(n+1) = V(n) - \frac{f(V(n))}{\dot{f}(V(n))}$$

where $V(n+1)$ is the next estimate. If $f(V(n+1))$ is sufficiently close to zero then calculations should terminate; if not, continue to iterate.

For the photovoltaic model, let

$$f(V) = 1 + \alpha V - e^{-\alpha(V_{oc}-V)}$$

The iteration formula then becomes

$$V(n+1) = V(n) - \frac{1 - \alpha V(n) - e^{-\alpha(V_{oc}-V(n))}}{\alpha - \alpha e^{-\alpha(V_{oc}-V(n))}}$$

A FORTRAN code was developed to implement this iterative procedure to determine the maximum power point for typical photovoltaic arrays. A source listing appears in Appendix A.

Form Factor

The form factor (a.k.a. fill factor or FF) is defined in a way that accounts for the maximum power in terms of the open circuit voltage and short circuit current. Let

$$P_{mp} = \text{FF } V_{oc} J_{sc} \tag{3.4}$$

and solving for FF gives defining equation

$$\text{FF} = \frac{P_{mp}}{V_{oc} J_{sc}}$$

A value for the form factor is generally available as a part of the manufactures specifications.

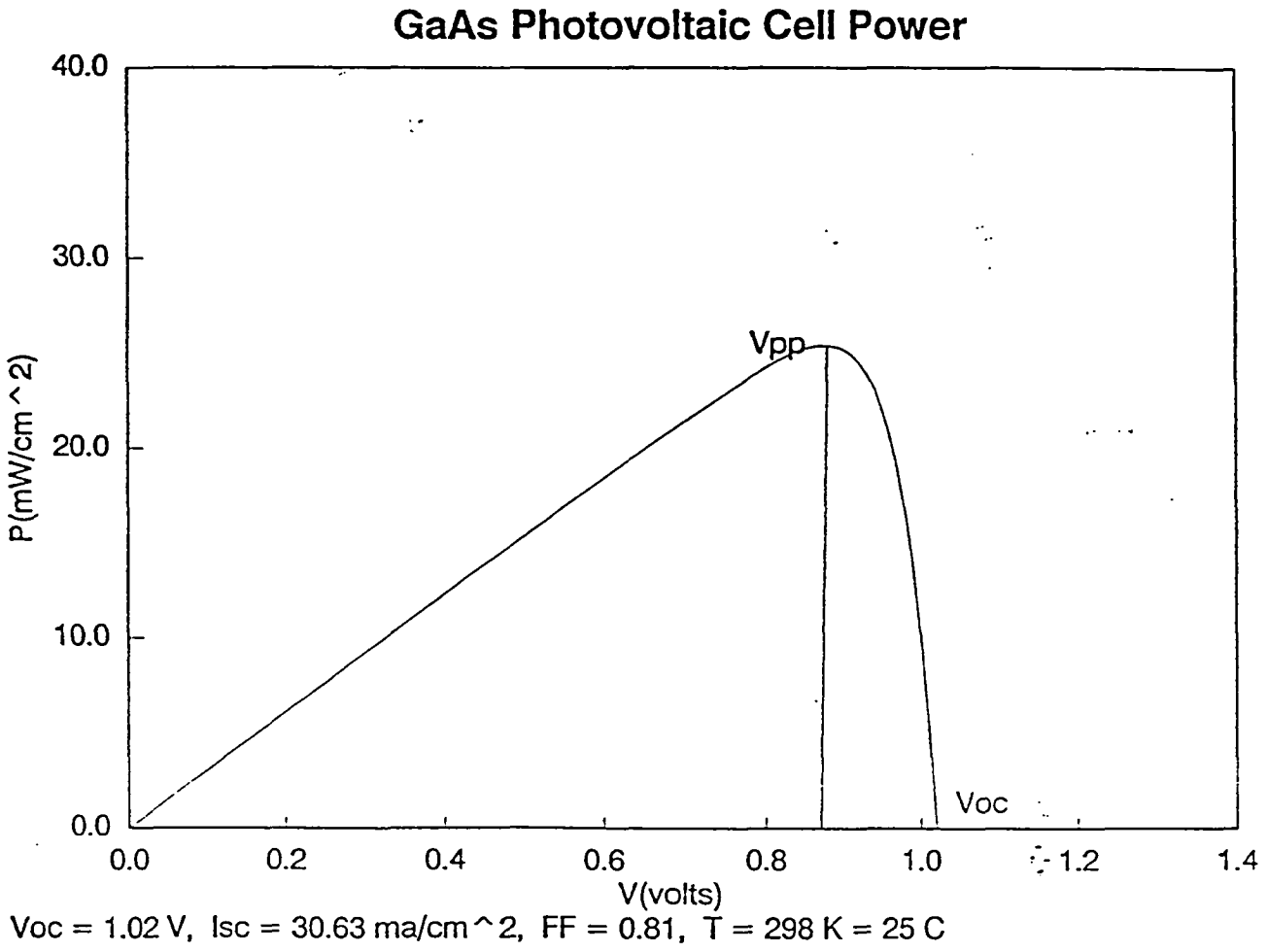

Figure 3.3: PVC Power Output

3.1.2 Photovoltaic Cell Temperature Sensitivity

The performance and electrical characteristics of photovoltaic cells depend upon the operating temperature in the vicinity of the semiconductor junction. Generally, as the junction temperature increases, the open circuit voltage decreases and the short circuit current increases. The shape of the characteristic current versus voltage curve (the $J-V$ curve) also changes with temperature affecting the maximum power output and fill factor. Typical examples of the J-V curve for a GaAs cell are depicted in Figure 3.4 for 173K and 423K junction temperatures.

The changes in cell parameters due to temperature tend to be constant over a fairly wide range of temperatures. The parameters are usually measured at a junction temperature of 25C, and are assumed to be constant. Values used as typical for GaAs cell are as follows:

$$\frac{\partial V_{oc}}{\partial T} = -1.9\text{mV/C}$$

$$\frac{\partial J_{sc}}{\partial T} = 20\mu\text{A/C}$$

Dependence of the maximum power output is usually expressed as a percent sensitivity, i.e. the maximum power is derated by a specified percentage for every degree increase in temperature. Mathematically, this sensitivity, S, can be expressed as

$$S_{P_{mp}:T} = (\frac{1}{P_{mp}})\frac{\partial P_{mp}}{\partial T} = -0.24\%/\text{C}$$

Relating P_{mp} temperature sensitivity to other model parameters can be derived by differentiating Equation 3.4 with respect to temperature (denoted by the superscript prime), or

$$P'_{mp} = \text{FF }'V_{oc}J_{sc} + \text{FF } V'_{oc}J_{sc} + \text{FF } V_{oc}J'_{sc}$$

This result can be solved to analytically determine the change in form factor with temperature, assuming constant $\partial P_{mp}/\partial T$,

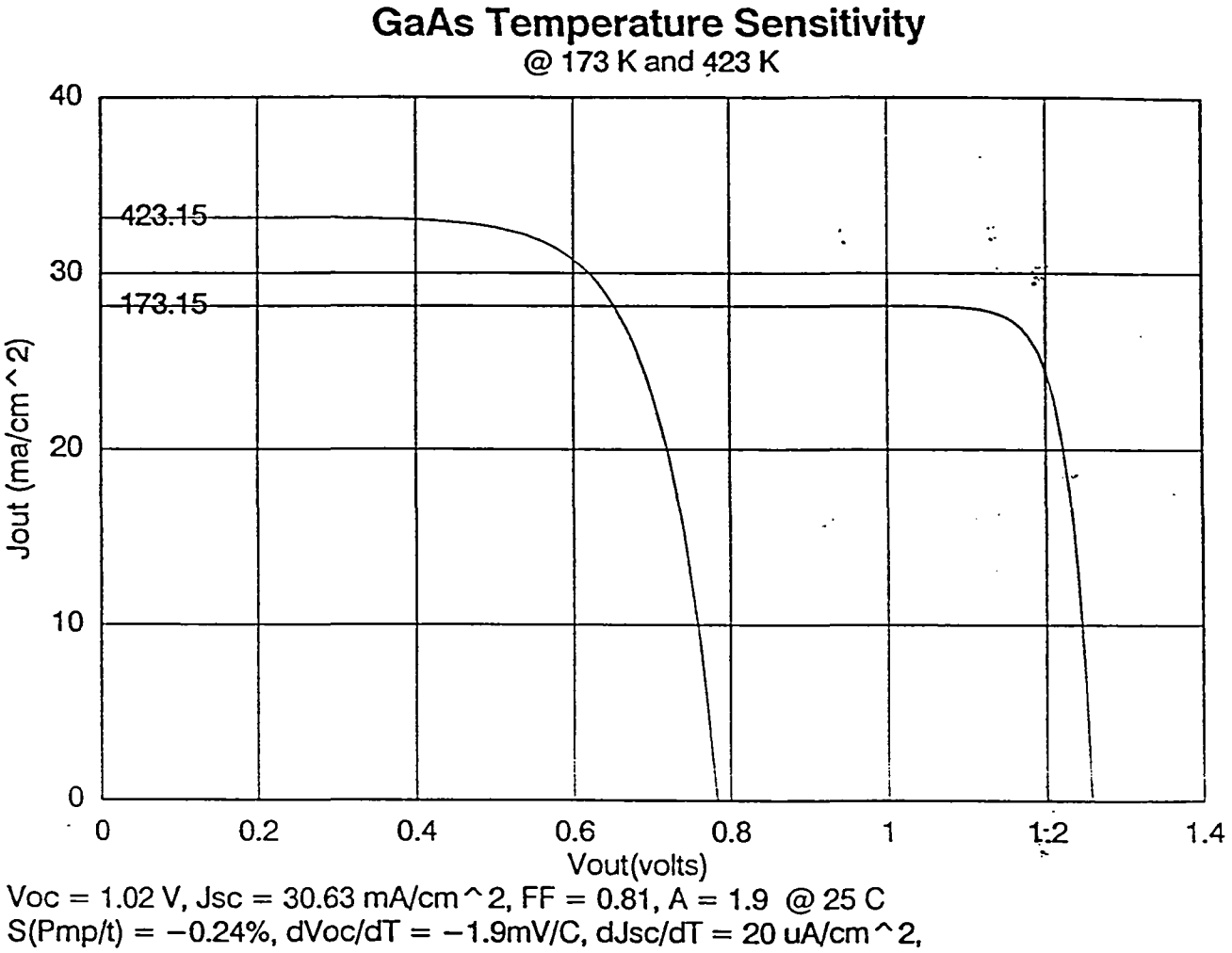

Figure 3.4: PVC J-V Curves at Temperature Extremes

$$\mathrm{FF}' = \frac{1}{V_{oc}J_{sc}}\left[P'_{mp} - \mathrm{FF}\ V_{oc}J'_{sc} - \mathrm{FF}\ V'_{oc}J_{sc}\right] \quad (3.5)$$

$$= -0.00096 \quad (3.6)$$

for the values listed above. Results for a cell temperature of 373K appears in Table 3.1. Note that values with a label including an equals sign, "=", are computed values, all others are input parameters.

Using this data and the Newton-Raphson method described in Section 3.1.1, the peak power voltage, V_{mp}, can be determined over a broad range of temperatures. The results of this analysis appear in Figures 3.5 and 3.6. The theoretical variation of V_{mp}, V_{oc}, and FF are plotted versus temperature over a range of −100C to +150C (173K to 423K).

3.2 Array model

A photovoltaic *string* refers to a number of individual cells connected in series. All strings are identical in the sense that they contain the same number of cells and as a result provide the same string operating voltage. The more cells that are connected in series, the higher the string operating voltage. String are connected in parallel to meet current demand. Connecting more strings in parallel uses a larger area of the array to produce power and increases available current. Cross linking string cells with corresponding neighbor string cells is not anticipated or considered.

The power system architecture regulates the number of strings supplying power in order to regulate the feed power from the arrays. This approach provides coarse control over the array bus voltage and functions to match generated power to power demand. Unused strings are left open.

GaAs Temperature Sensitivity Analysis (T = 173 - 423)

AM0	136.8 mW/cm^2	T(K) =	298 24.85 C
Voc @25C	1.020 V	Voc @T	1.020285
Jsc @25C	30.630 mA/cm^2	Jsc @T	30.627
FF @25C	0.810	FF	0.810145
Pmp =	25.307 mW/cm^2	Pmp =	25.31562
eta	18.50%	eta	18.51%
dPmp/dT=	-0.06074 mW/cm^2/C	S(Pmp/T)	-0.24%
dVoc/dT	-1.9 mv/C	S(Voc/T)=	-0.19%
dJsc/dT	20.0 uA/cm^2/C	S(Jsc/T)=	0.07%
dFF/dT	-0.00096	S(FF/T) =	-0.12%

check: using Pmp = FF*Voc*Jsc

dPmp/dT = [FF Voc J'sc + FF V'oc Jsc + FF' Voc Jsc]	-0.06074
dVoc/dT = [P'mp - FF Voc J'sc - FF' Voc Jsc] / (Jsc FF)	-0.0019
dJsc/dT = [P'mp - FF V'oc Jsc - FF' Voc Jsc] / (Voc FF)	0.02
dFF/dT = [P'mp - FF Voc J'sc - FF V'oc Jsc] / (Voc Jsc)	-0.00096

Table 3.1: PV Cell Temperature Sensitivity Analysis

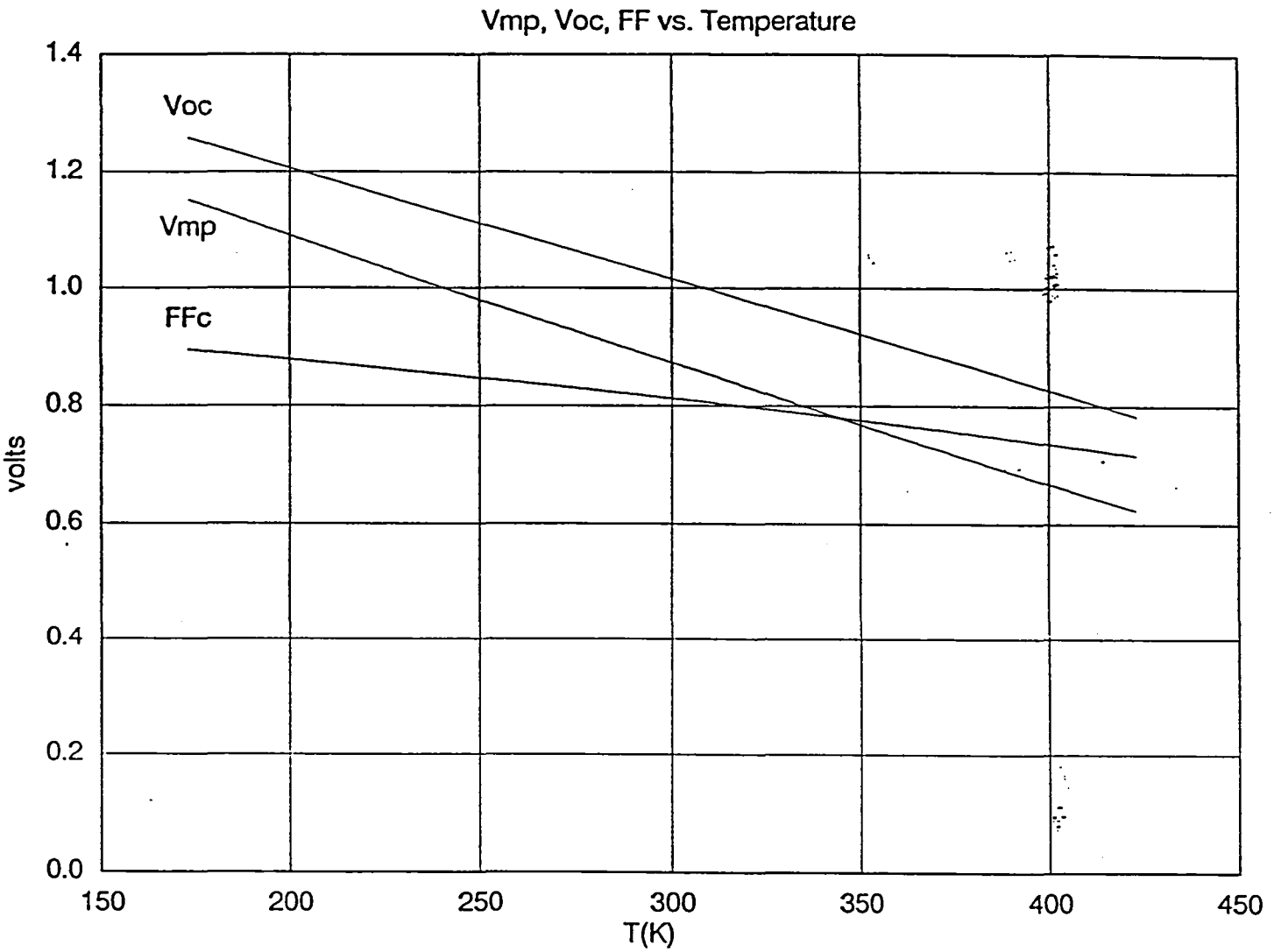

Figure 3.5: PV Cell Voltage Parameters versus Temperature

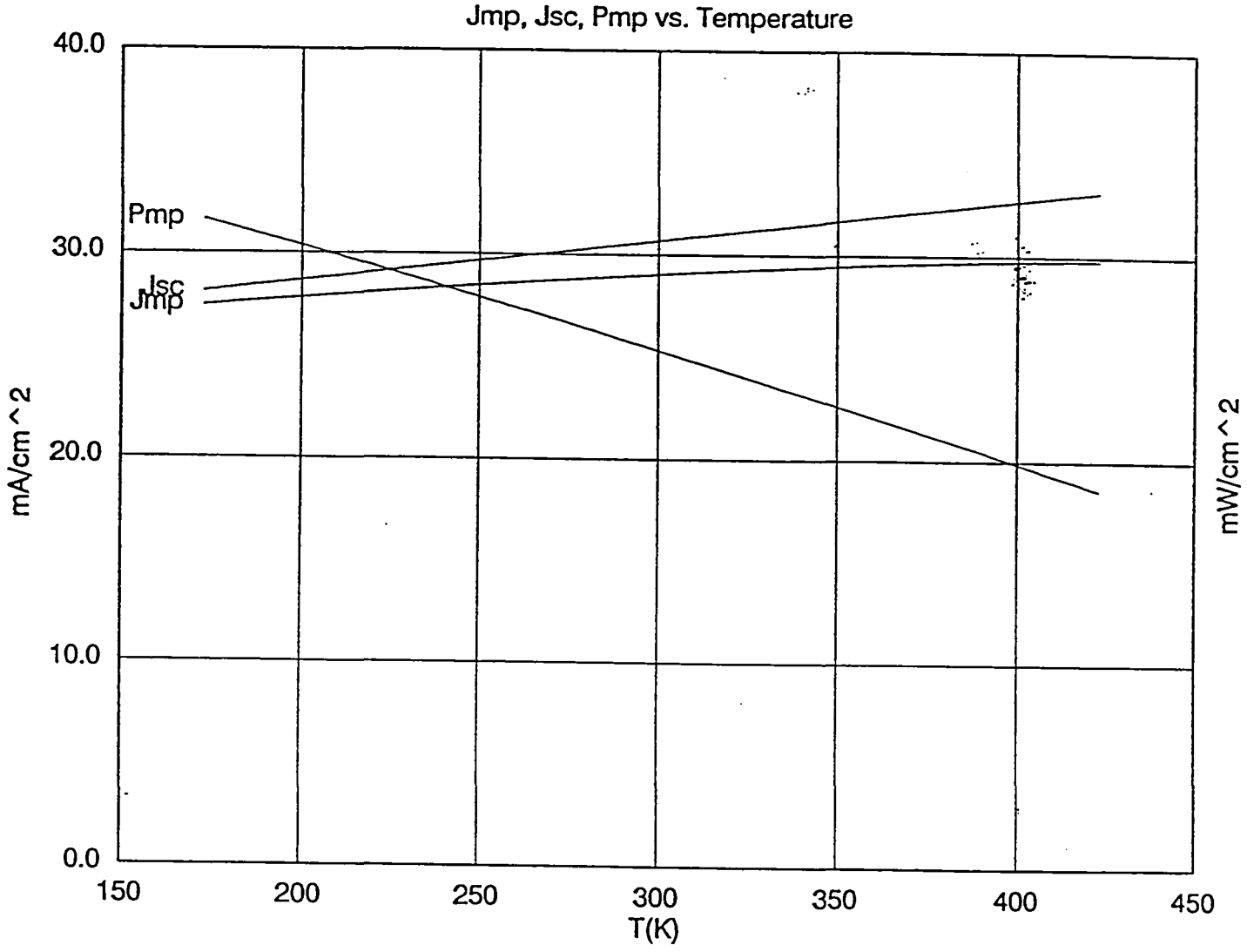

Figure 3.6: PV Cell Current Parameters versus Temperature

Extending the photovoltaic cell model in Section 3.1 to account for series and parallel connections appears in JPL Solar Cell Handbook. Ignoring the effects of series resistance in the cell, gives

$$I = N_p I_{sc} \frac{\left(e^{\frac{V_{oc}}{V_{th}}} - e^{\frac{V}{N_s V_{th}}}\right)}{\left(e^{\frac{V_{oc}}{V_{th}}} - 1\right)}$$

where N_s is the number of cells connected in series to form a string, and N_p is the number of strings connected in parallel.

Figure 3.7 contains a typical I-V curve for an array.

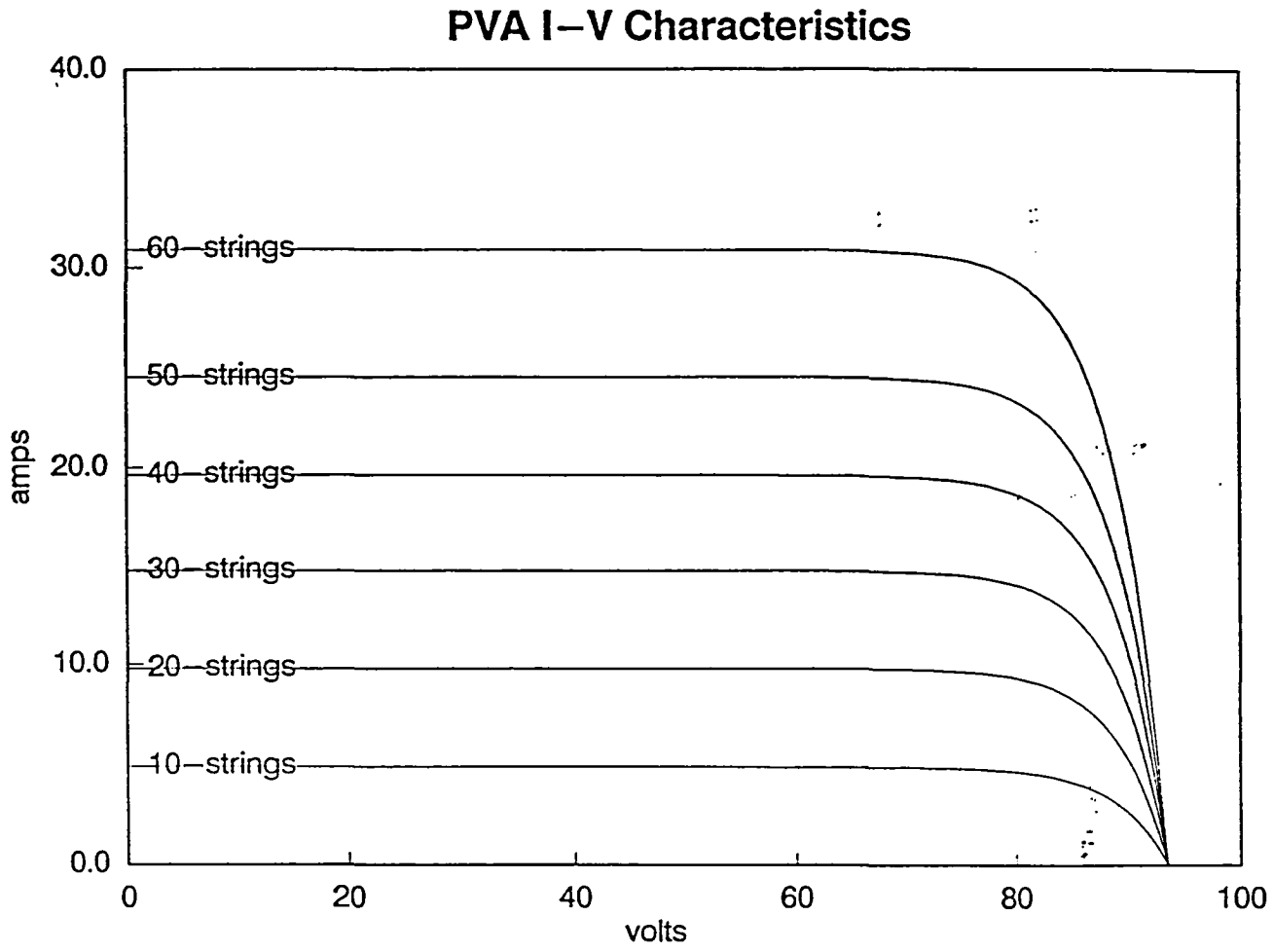

Figure 3.7: PVA I-V Characteristics

Chapter 4

Architecture

The power management and distribution system controls the flow of energy among the photovoltaic array, the thrusters, the battery and the loads. A top level depiction of this architecture and its relationship to the photovoltaic arrays, propulsion, batteries, and loads appears in Figure 4.1. PMAD consists of five functional subsystems:

1. a microprocessor based power regulation unit (PRU),
2. a power conversion unit (PCU) using a reverse polarity buck/boost topology,
3. a battery charge controller (BCU),
4. a battery discharge controller (BDU),
5. a power distribution unit (PDU) including the load voltage regulators.

The most significant feature of this architecture is its unique application of the buck/boost topology to solve plasma interaction problems without additional complexity, dissipation or weight. A simple grounding scheme is maintained that does not require isolation.

The buck/boost power conversion unit, changes the sign of the input voltage with respect to the output voltage. This feature of buck/boost convertors allows the photovoltaic array to be positive grounded (and take advantage to

the resulting reduction in spacecraft charging effects), and provide a negative ground power supply to the loads.

Battery charge electronics have been selected to provide high, but current limited, initial charge rates. Full charge sensing automatically switches the battery charger into a trickle charge mode without overcharging.

The battery discharge controller was selected to provide high efficiency conversion with well regulated output voltage. This strategy minimizes conversion losses during discharge cycles, and losses associated with the load voltage regulator. By maintaining a stable discharge controller output voltage, a minimum dropout voltage across the load voltage regulator can be maintained.

The scientific instrument load on TROPIX requires a well regulated 28 volt power supply which is quiet. Switching transients associated with switch mode power supplies must be blocked prior to distribution among these loads. In the power distribution unit, an analog voltage controller was selected for this purpose. Its design is simple and reliable with excellent noise rejection properties. However, analog regulators are dissipative which reduces efficiency and increases the heat load.

The mathematical models used to analyze the current and voltage features of the photovoltaic array appear in Section 3. The electronic configuration of the arrays and the sequential string control strategy is discussed in Section 4.4.1.

4.1 Electric Thruster Interface

The electric thrusters used on this vehicle have integral power processing units (PPUs) which develop the necessary internal supplies. Current PPU designs require a nominal 80 volt DC input. Since this is a high enough voltage to take substantial advantage of the wiring harness mass reduction, the array bus voltage was selected to be 80 volts.

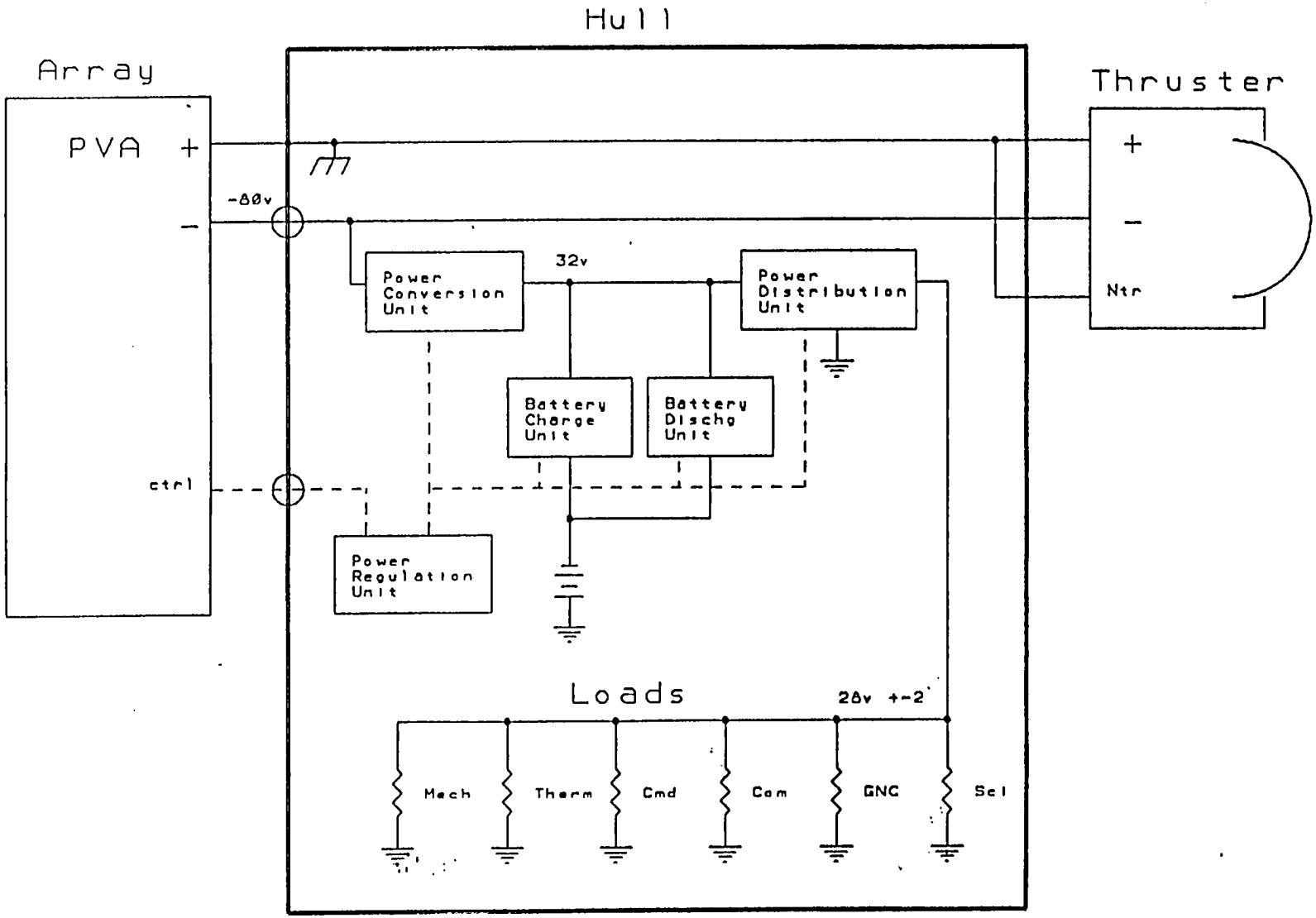

Figure 4.1: TROPIX Power System Architecture

The input voltage to the thruster PPUs is acceptable over a rather broad range (60-100 volts). Power is delivered directly from the photovoltaic array using only sequential string switching to control this input voltage. This approach provides sufficient regulation for the thruster PPUs and relieves the power conversion from handling this power flow. Since the thrusters constitute a large percentage of the total vehicle electric load, this results in a substantial savings in weight, and dissipation.

4.2 Photovoltaic Array Configuration

Figure 4.2 contains a schematic representation of the electronic configuration of the photovoltaic array. Photovoltaic cells, wired in series to generate the desired array output voltage, are the array strings. Several strings are connected in parallel to supply the demand current. Series FETs control whether current can flow through an individual string. Blocking diodes prevent reverse currents from flowing through dark (or shorted) strings. Select GaAs cells may allow array designers to eliminate these devices.

The series n-channel FET pass transistors control the current flow through each string with very little dissipation. Typical on resistances for currently available devices are less than 0.1 ohm. For an array using 4 cm x 4 cm cells, the current produced by a string is about 450 mA, which means that approximately 20 mW is lost, which is substantially less than the 300 mW loss associated with the blocking diodes.

A tradeoff study was performed to show the effects of photovoltaic array operating voltage on wiring harness weight for 28, 56, and 112 volts. The results of this study indicate there is a considerable savings in mass as the array goes to higher voltages. Other factors influenced the choice of PVA operating voltage.

Current thruster PPU designs require 80 volts DC input (nominal). This voltage is high enough to take substantial advantage of the wiring harness mass reduction, and relieves the power conversion unit from handling this load. The array bus voltage was selected to be 80 volts.

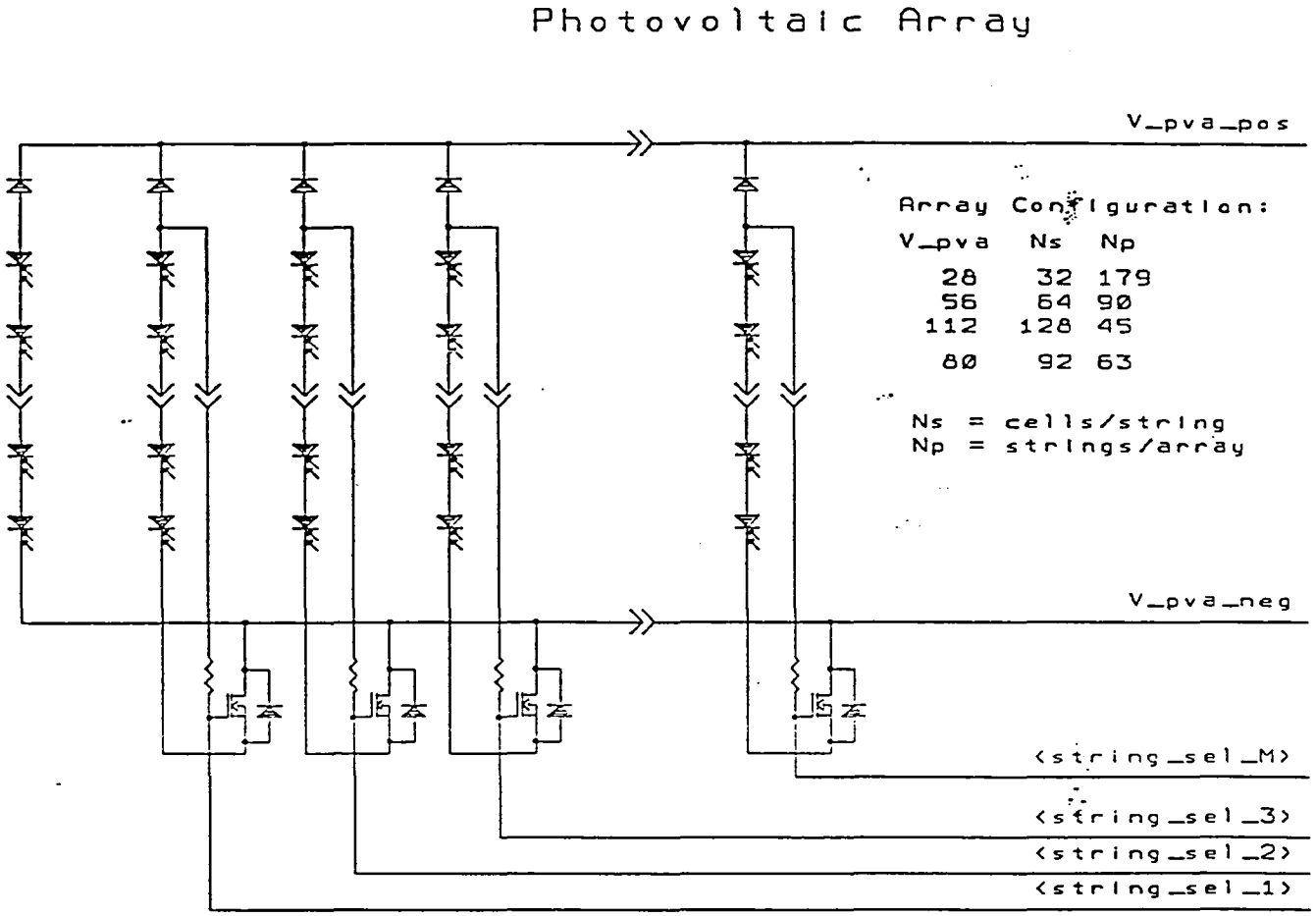

Figure 4.2: PVA Schematic

4.3 PVA String Analysis

An analysis was conducted to determine the number of photovoltaic cells wired in series, N_s, to form a string under nominal operating conditions experienced by the arrays while in orbit. The number of strings, N_p, was then determined by dividing the total number of cells, N_t, by the number of strings. A Lotus 123 spreadsheet was developed to perform this analysis and is provided on magnetic media as a part of this report. Table 4.1 contains the results of this analysis.

Note that the peak power point has been determined by assuming that the form factor is split between the open circuit voltage and the short circuit current. Since

$$P_{mp} = \mathrm{FF}\ V_{oc} J_{sc}$$

and by dividing the influence of the form factor between V_{oc} and I_{sc} this equation can be rearranged to yield,

$$P_{mp} = (\mathrm{FF}^{(1-\gamma)} V_{oc})(\mathrm{FF}^{\gamma} J_{sc})$$

where,

$$\gamma = 0.25$$

The value for gamma was determined from peak power data presented in Figure 3.6. This simplification is a reasonable first pass estimate and sufficient for computations regarding array configuration issues.

4.4 Power Regulation Unit

The Power Regulation Unit is a microprocessor based system responsible for controlling the power exchanged among the spacecraft loads and systems. The microprocessor specifically senses array voltage and responds by adding or removing PVA strings accordingly. The microprocessor also monitors load voltage, battery charge and discharge rates and applies appropriate controls.

TROPIX -- PVA Configuration

CELLS			WINGS	
Voc	1.020	V	wing area	6.130 m^2
conv efficiency	0.185		packing factor	0.75
FF	0.81		solar insol AM0	1368 W/m^2
L x W	4 4	cm x cm	power per panel =	1163.54 W
T(K)	298.15			
Jsc =	30.63	mA/cm^2		
Isc =	490.11	mA	ARRAY	
Voc * Isc =	0.4999	W	# wings	2
Vpp = Voc*FF^0.75	0.872	V	total area =	12.260
Ipp = Isc*FF^0.25	464.210	mA	total power out =	2327.07 W
Pmax =	0.4049	W	total cells (Nt) =	5747

Isc = Irb(exp(Voc/Vth)-1)

ARRAY Constitutive Equation

I = Np Isc (exp(Voc/Vth) - exp(V/(Ns Vth)))/(exp(Voc/Vth) - 1)

BUS VOLTAGE	ARRAY CURRENT	cells/ string	string/ array	total cells
		Ns	Np	Nt
28 V	83.1 A	32	179	5747
56 V	41.6 A	64	90	5747
112 V	20.8 A	128	45	5747
80 V	29.1 A	92	63	5747

Table 4.1: PVA Configuration Analysis

4.4.1 PVA Control

Control of the photovoltaic array is necessary to in order to match the power supplied from the array to the load demand. Sequential switching of array strings is used to accomplish this and provides coarse control over the input voltage to the power conversion unit and the electric thrusters. This approach minimizes the heat load inside the spacecraft and consequently the thermal dissipation which must be handled by the thermal control system.

Since the integral power processing unit for the electric thrusters can tolerate a rather large range of input voltages, sequential string switching provides more than enough regulation for the propulsion load. The strategy is as follows.

When the array voltage is reduced to a minimum threshold voltage as a result of either decreased solar insolation or increased load, the microprocessor detects the condition and commands additional series FET switches to be turned on. This connects additional strings to the PVA bus, increasing available current and bus voltage. If the load decreases, bus voltage will increase until an upper threshold is reached, at which point the controller will reduce available current by turning of a series FET. A software implemented Schmidt Trigger algorithm will be used to prevent jitter and oscillation when operating in the vicinity of a threshold. This strategy is depicted in Figure 4.3 and provides coarse control over the PVA bus voltage.

There are known stability and array voltage collapse problems with sequential switching of photovoltaic arrays used in conjunction with switching power conversion units. These problems can be avoided if the array operating voltage is kept well above the maximum power point. By carefully selecting the threshold points, operations in the stable region above the maximum power point can be guaranteed.

4.4.1.1 PVA Sequential String Switching

The flow of energy from the arrays is matched to the load using a sequential string switching strategy. As demand increases or solar insolation decreases,

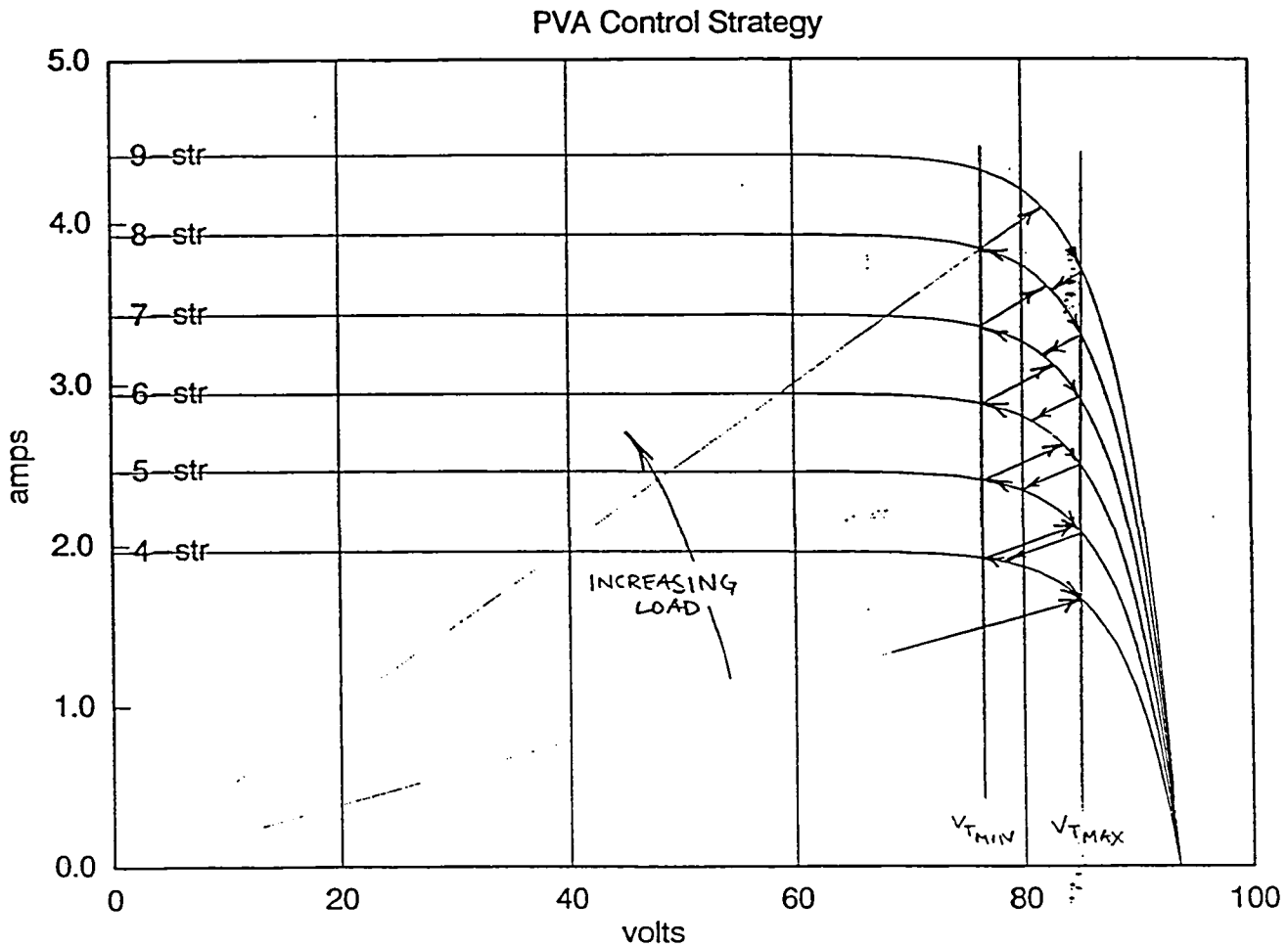

Figure 4.3: I-V Control Strategy

the output voltage from the array begins to sag. String switching is accomplished using high performance field effect transistors (FETs) in series with each string. The schematic representation in Figure 4.2 depicts the control signals driving the gate terminal of the FET switches.

4.4.1.2 PVA String Controller

The PVA string controller performs several functions vital to the overall power system function. The string controller provides coarse control over the PVA bus voltage in order to provide power within the allowable range to the thruster power processing units and power conversion unit. The microprocessor can also provide for sophisticated self test, string scheduling and reconfiguration, and diagnostic capabilities using microprocessor diagnostic software.

Figure 4.4 depicts the electronic configuration of the PVA control electronics. Serial communications from the microprocessor to the wing mounted control electronics minimize the number of wires which must cross the array boom gimbals. Optical coupling is depicted here although an arrangement with slip rings or similar device would probably be acceptable. Assuming an eight bit control word, there are 256 different combinations of energized strings. During normal control operations, strings can be energized according to the following scheme:

Using another 32 of these states, strings can be selected one at a time for self test purposes:

The remaining states can be used for various other combinations of strings for self test and control. The kind and sophistication of self test and diagnosis programs which could be implemented using the PRU control microprocessor are virtually limitless. It is technically possible to test the I-V characteristics for each individual string. This kind of information may herald impending failure or reduced output. Weak or failing strings could potentially be identified, and the control strategy adjusted accordingly, prior to a catastrophic failure. Shorted strings which could potentially cause overall power system failure could be identified and locked out. Peak power points for each individual string could be determined in real-time by simultaneously sensing

Control Word	String Select Active
0	none
1	1
2	1, 2
3	1, 2, 3
4	1, 2, 3, 4
5	1, 2, 3, 4, 5
6	1, 2, 3, 4, 5, 6
...	...
32	1 thru 32

Table 4.2: String Select Decoding - Normal Operations

Control Word	String Select Active
224	none
225	1
226	2
227	3
228	4
...	...
255	32

Table 4.3: String Select Decoding - Self Test Operations

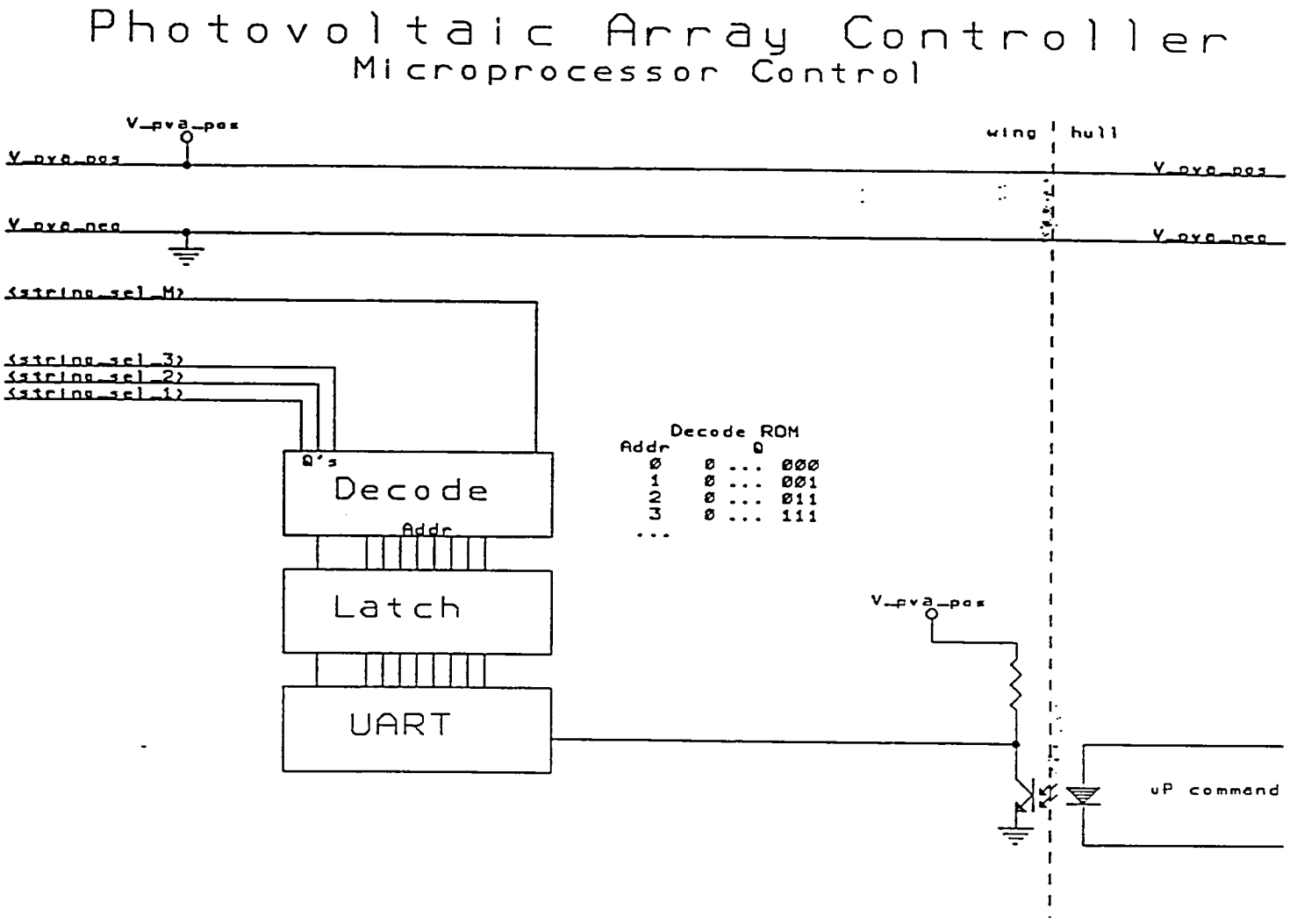

Figure 4.4: Power Regulation Unit - PVA Interface

string voltage and current as a variable load is applied.

While the architecture presented here allows for flexible use of power system assets, further study to develop detailed strategies are needed. Reliability and fault tree analysis will no doubt provide considerable insight as to the extent this self test and diagnosis function should be implemented.

For instance, if it were desirable to be able to select all possible combinations of the 32 strings on a wing, then 4 eight bit word could be latched, giving a total of 32 control bits. Each control bit could be used to activate the corresponding string. A flexible control strategy could then be used which would avoid failing strings, reducing the effects of aging on individual strings.

4.5 Power Conversion

The power conversion unit selected is a unique solution to the plasma interaction problem experienced by spacecraft in low earth orbit. This is accomplished, using a reverse polarity buck/boost topology, without additional complexity, dissipation or weight. A simple grounding scheme is maintained that does not require isolation. A description of this phenomenon follows.

A buck/boost power conversion unit, changes the sign of the input voltage with respect to the output voltage. This topology is usually employed to convert a positive voltage into a negative voltage. A reverse polarity buck/boost convertor, however, does the opposite; converting a negative voltage input into a positive voltage. This feature of a reverse polarity buck/boost convertors allows the photovoltaic array to be positive grounded (and take advantage to the resulting reduction in spacecraft charging effects), and provide a negative ground power supply to the loads. A schematic of this implementation appears in Figure 4.5 .

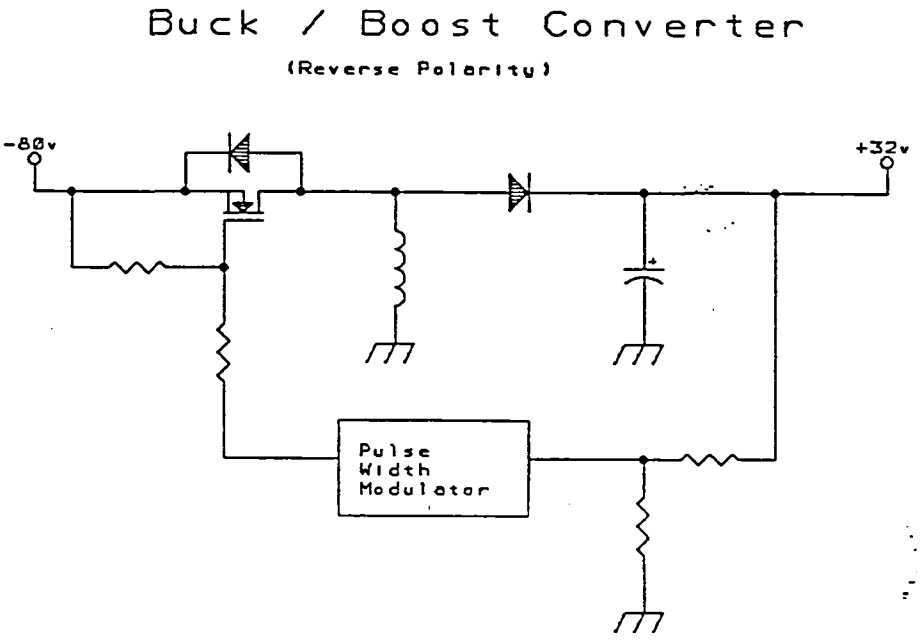

Figure 4.5: Power Conversion Schematic

4.6 Battery Charging

By initially limiting the power flow to the battery during a charge cycle, overcharging and overheating can be prevented. For a battery capacity of C_{batt} (W-hr), the energy flow limit was selected to be 58% of the capacity or

$$\begin{aligned} P_{\text{max}} &= 440 \text{ (W-hr)}/1.72 \text{ (hr)} \\ &= 256 \text{ (W)} \end{aligned}$$

This implies that the maximum charging current is limited to

$$\begin{aligned} I_{\text{max}} &= C_{\text{batt}}(\text{W-hr})/1.72 \text{ (hr)}/V_{\text{batt}}(\text{V}) \\ &= 9 \text{ (A)} \end{aligned}$$

As the battery charges, the battery terminal voltage increases. When the terminal voltage has increased to 1.33 volts per cell, or 31.9 volts the battery is fully charged and the charger switches from current limit mode to a float voltage mode. This mode maintains the battery state of charge near 100% by providing a fixed voltage of 1.25 volts per cell, or 30.0 volts.

Figure 4.6 depicts the schematic for the battery charge electronics. The circuit functions in this way:

> The SCR is initially open leaving no current path from the LM117 ADJ terminal to ground. The LM117 acts as a current source under these conditions. Current flowing through R7 drives Q1 into the active region sourcing current to pass transistor Q2.
>
> Voltage division at the SCR gate prevents triggering until the battery reaches full charge at 31.9 volts. When the SCR is triggered, a current path to ground for R2 is provided. The LM117

acts as a voltage source at this point providing a float voltage of 30.0 volts at the battery terminals which maintains a trickle charge until V_{dd} drops below 32.4 volts.

Diodes D2 and D3 protect the LM117 when the input voltage drops rapidly. Zener diode, D4, provides crowbar protection in the event that V_{dd} exceeds about 40 volts.

4.7 Battery Discharging

Battery discharge electronics are implemented using a boost convertor topology depicted in Figure 4.7. The load voltage regulator, which is driven by the discharge convertor, is an analog regulator with approximately a 2 volt dropout, and requires 32 volt input in the worst case. The boost convertor can provide a high efficiency (92%) drive with good regulation over the entire range of battery discharge voltages.

The maximum demand from the loads during battery discharge cycles is 307 W and 28 volts or about 11 amps.

4.8 Power Distribution Unit

The power distribution unit consists of a load voltage regulator and terminations for the various load power wiring. The primary function of the load voltage regulator is to provide low noise, regulated DC power to the loads.

The switching transients created by the power conversion unit and the battery discharge unit must be blocked prior to distribution among the loads. The scientific instruments, in particular require a 28 volt power supply which is well regulated and quiet. Switching transients are sufficiently fast to radiate EMI which can interfere with sensitive electronics and sensors. An analog voltage controller with current boost was selected for this purpose. The design, depicted in Figure 4.8, is simple and reliable with excellent noise rejection properties and relatively low dropout (about 4 volts).

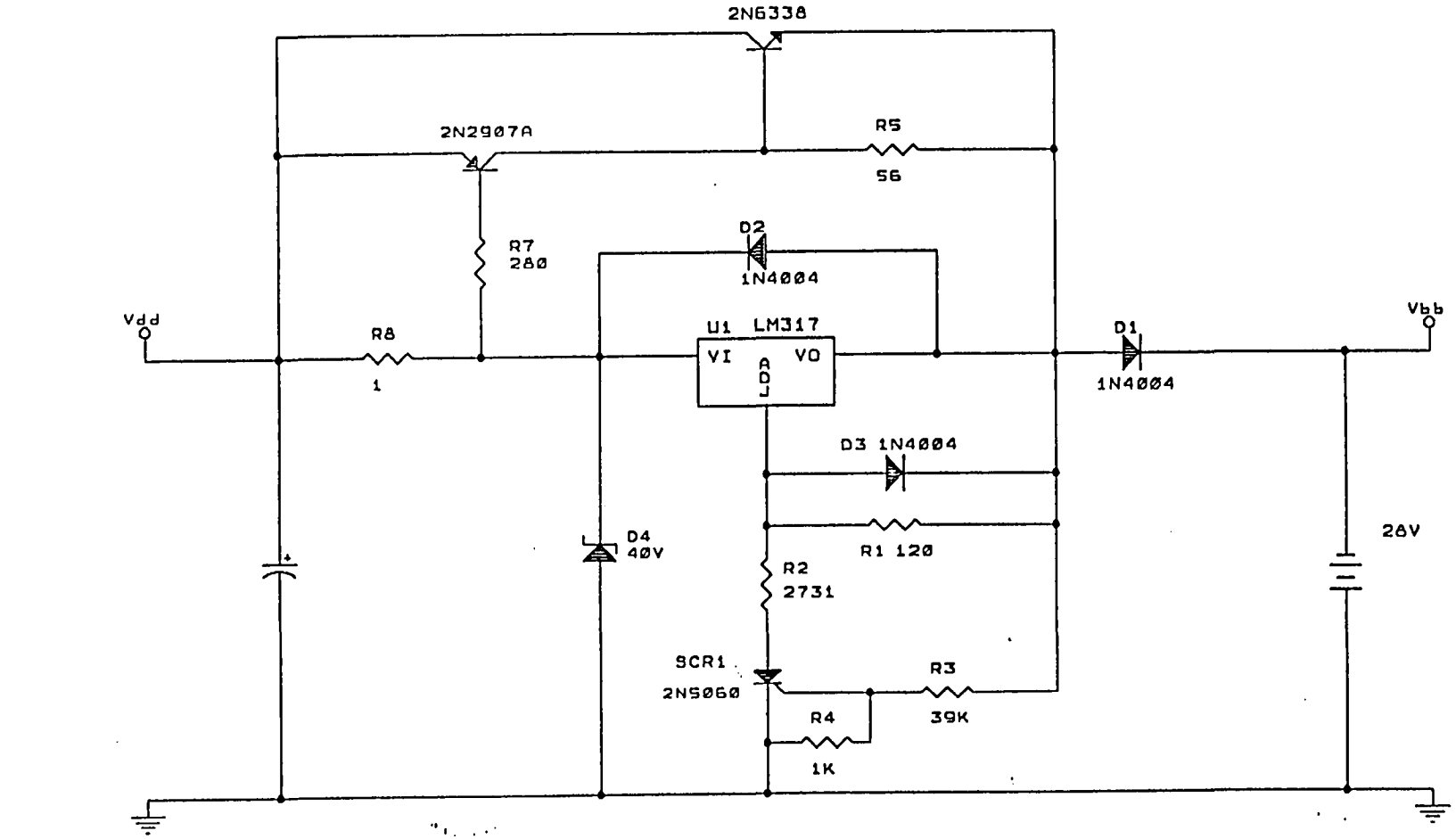

Figure 4.6: Battery Charger Schematic

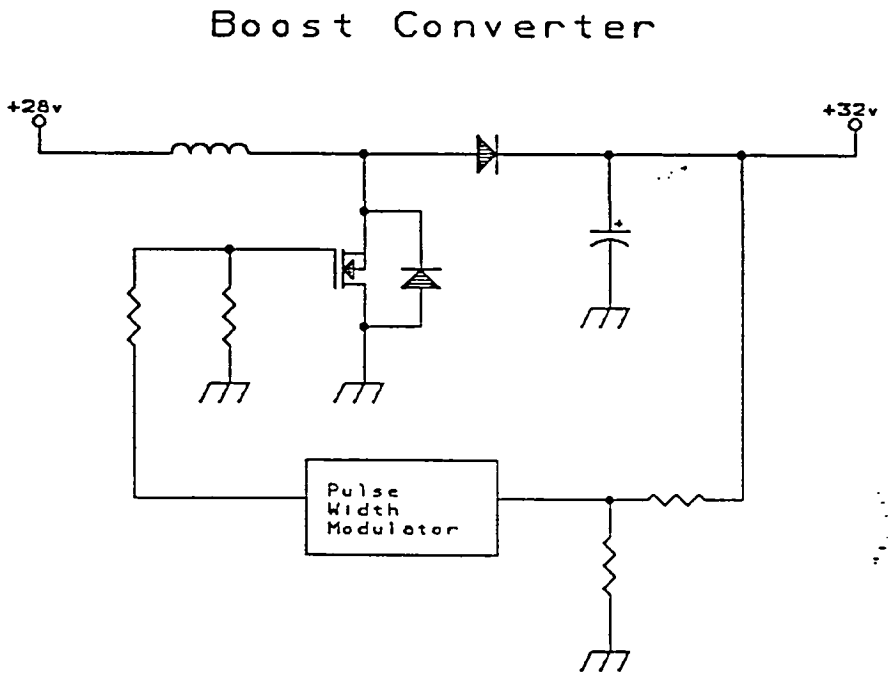

Figure 4.7: Battery Discharge Schematic

Analog regulators are dissipative which reduces efficiency and increases the heat load. Placing this unit close to the power conversion unit and the battery discharge unit will minimize the radiated components caused by switching transients.

The circuits functions as follows:

> An input Pi network (L1, C1, C2) is tuned to suppress switching transients at the fundamental frequency (20KHz). Sense resistor R1 develops a voltage drop of 0.6 volts when approximately 300 mA flows into regulator U1 (LM117). This provides a sink for base current from the PNP pass transistor (Q1). Q1 begins to conduct and provide source current to NPN pass transistor Q2. Additional load current demand will cause the sense resistor voltage to increase and cause pass transistor Q2 to source a larger share of the load current. Programming Resistors R4 and R5 are selected to provide 28 VDC at the output. Capacitor C3 provides additional supply decoupling.

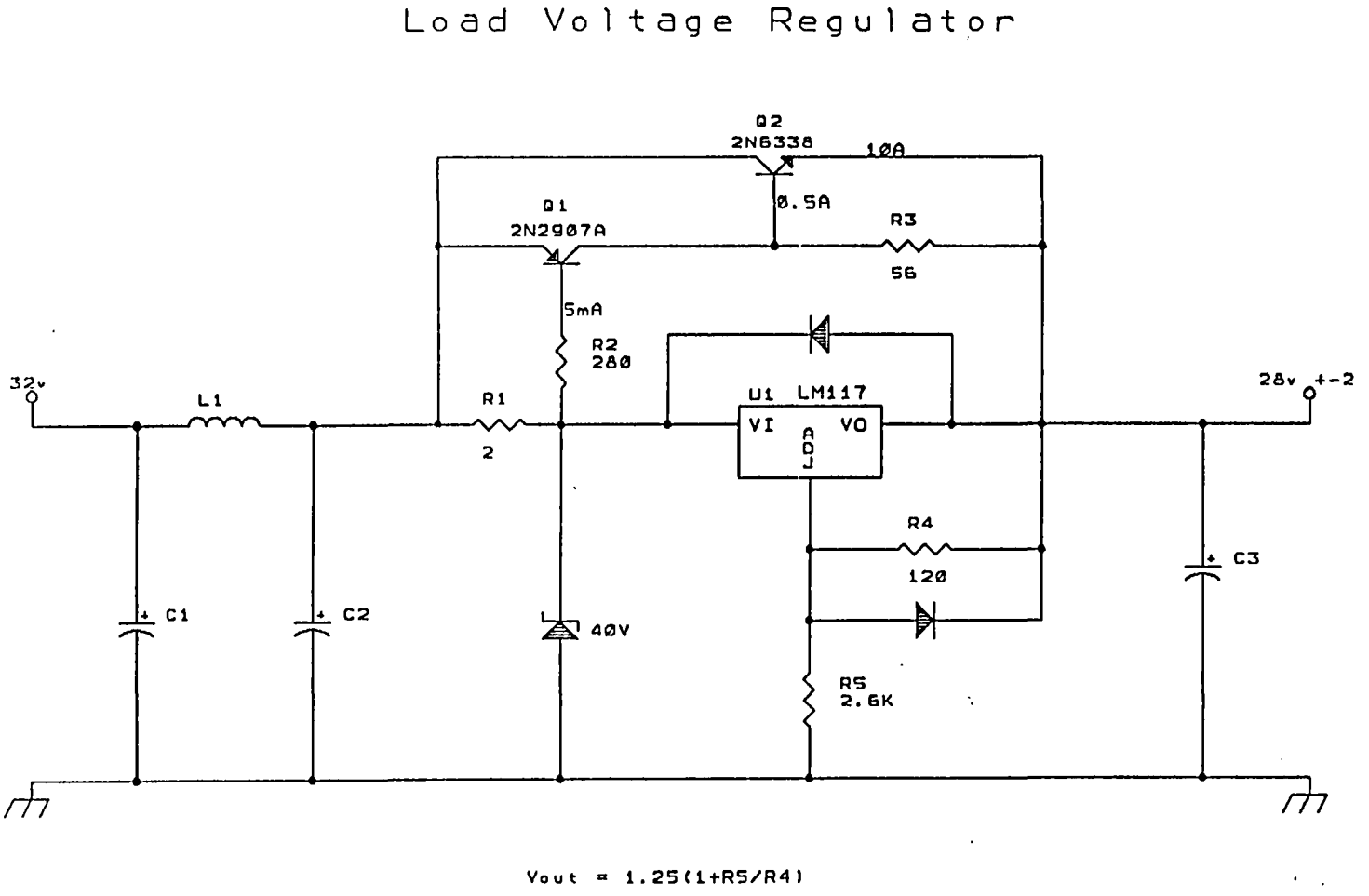

Figure 4.8: Power Distribution Unit

Chapter 5

Mass and Volume Estimates

Mass and volume estimates are presented in the sections that follow. Estimates are presented for power regulation, power conversion, battery charger, battery discharger, and power distribution. An overall mass budget for the PMAD less battery is 26.3 KG. Tables 5.1 and 5.2 contain the PMAD system volume and mass rollups, which are also available on magnetic media.

5.1 PVA Harness

The PVA wiring harness conducts electrical power from the photovoltaic array to the PMAD. For the purpose of estimating the mass of this wiring harness, it is assumed that each photovoltaic panel has a separate pair of insulated conductors, one for supply current and the other for return current. Harness mass is dependent upon the operating voltage of the photovoltaic array. For an array operating at a fixed output power, higher operating voltages reduce the current flow required to deliver the power. Since ampacity (the current carrying capacity of a conductor) is limited by the cross sectional area of the conductor, considerable mass savings can be achieved by operating the array at as high a voltage as practical.

Mass and losses are estimated for operating voltages of 28, 56, 112 volts. Mass and losses at an operating voltage of 80 volts (the thruster operating voltage) are also included. Conductors of copper and aluminum were considered at

current densities of 700 and 400 circular mils per amp.

Table 5.3 lists the relevant parameters used to determine the required wire size. The wire gauge selection process considered even numbers from 0 to 22 AWG. Conductor gauge was determined by selecting the closest cross sectional area which exceeded the required area. The notation, "c_m" refers to circular mils, the most common unit of area found in the published wire tables. A circular mil is the area of a circle which is one mil (thousandth of an inch) in diameter.

These results appear in Table 5.4 with the corresponding wire properties. An estimate of harness weight and electrical losses, based on the selected gauge and properties, was computed. Tables 5.5, and 5.6, present these mass, electrical resistance and loss estimates in tabular form, for the cable runs in Table 5.7.

The wiring harness run lengths were estimated from spacecraft blueprints. Each current supply/return pair is assumed to run from the center of a 61 cm by 126 cm panel attached to a central gimbaled boom. Each of the two wings is composed of 8 panels. The PMAD is assumed to be located on the baseplate near the thrusters. Details of the run length associated with each panel appears in Table 5.7.

The wiring harness mass plotted versus PVA operating voltage appears in Figure 5.1.

Mass and Volume Estimates

		kg	cm	cm	cm	vol	g/vol
PRU	Power Regulation Unit	7.0	20.0	21.0	20.0	8400	0.833
PCU	Power Conversion Unit	4.8	15.0	20.0	20.0	6000	0.800
BCU	Battery Charger Unit	2.7	10.0	16.0	20.0	3200	0.844
BDU	Battery Discharge Unit	2.7	10.0	16.0	20.0	3200	0.844
PDU	Power Distribution Unit	7.0	20.0	38.0	20.0	15200	0.461
PRO	Propulsion Harness	1.5					
		======				=======	
	estimate	25.7				36000	
	target	26.3					

Table 5.1: PMAD Mass and Volume Estimates

PRU	Power Regulation Unit	7.0
		======
	- Microprocessor	2.0
	- Array Bus Voltage Sense	0.3
	- String Control	2.8
	- Array Power Wiring	1.4
	- Array Power Interconnect	0.5
PCU	Power Conversion Unit	4.8
		======
	- Buck/Boost Convertor	3.8
	- Wiring Harness	0.5
	- Interconnect	0.5
BCU	Battery Charge Unit	2.7
		======
	- Dual Mode Charger	2.2
	- Wiring Harness	0.3
	- Interconnect	0.2
BDU	Battery Discharge Unit	2.7
		======
	- Boost Convertor	2.2
	- Wiring Harness	0.3
	- Interconnect	0.2
PDU	Power Distribution Unit	7.0
		======
	- Load Voltage Regulator	3.4
	- Load Wiring Harness	0.5
	- Load Interconnect	3.1
PRO	Propulsion Harness	1.5

Table 5.2: PMAD Subsystem Mass Estimates

PVA BUS -- WIRE HARNESS MASS AND ELECTRICAL LOSS ESTIMATE

PARAMETERS

PANELS				rho	resist
L x W	61	126 cm x cm		gm/cm^3	uohm-cm
power		143.75 watts	Cu	8.890	1.742
			Al	2.703	2.828
WING					
# panels/wing		8			
power		1150			
ARRAY			c_m/amp		cm^2/amp
# wings		2	700		0.00355
power		2300 watts	400		0.00203
Trial bus voltage		80	note:	5E-06 cm^2/c_m	

Table 5.3: PVA Bus Wiring Harness Parameters

PVA BUS -- WIRE HARNESS MASS AND ELECTRICAL LOSS ESTIMATE

GAUGE SELECTION

PVA volts	load amps	c_m/amp	min. c_m	Select AWG	c_m
28	5.134	700	3594	14	4106
56	2.567	700	1797	16	2583
112	1.283	700	898	20	1021
80	1.797	700	1258	18	1624
28	5.134	400	2054	16	2583
56	2.567	400	1027	18	1624
112	1.283	400	513	22	643
80	1.797	400	719	20	1021

WIRE PROPERTIES

PVA volts	AWG	Insul. gm/cm	Cu Cond. gm/cm	Cu Total gm/cm	Cu ohm/cm	Al Cond. gm/cm	Al Total gm/cm
28	14	0.05909	0.1850	0.2441	8.4E-05	0.0562	0.1153
56	16	0.04736	0.1163	0.1637	1.3E-04	0.0354	0.0827
112	20	0.03584	0.0460	0.0818	3.4E-04	0.0140	0.0498
80	18	0.04009	0.0732	0.1132	2.1E-04	0.0222	0.0623
28	16	0.04736	0.1163	0.1637	1.3E-04	0.0354	0.0827
56	18	0.04009	0.0732	0.1132	2.1E-04	0.0222	0.0623
112	22	0.03356	0.0289	0.0625	5.3E-04	0.0088	0.0424
80	20	0.03584	0.0460	0.0818	3.4E-04	0.0140	0.0498

Table 5.4: PVA Bus - Gauge Selection and Wire Properties

PVA BUS -- WIRE HARNESS MASS ESTIMATE

HARNESS MASS & LOSS -- COPPER CONDUCTORS -- 700 c_m/amp

PVA volts	AWG	cond. mass gm	insul. mass gm	total mass gm	total resist ohm	power loss watts
28	14	2075.67	663.06	2738.73	0.9395	24.76
56	16	1305.52	531.43	1836.95	1.4937	39.37
112	20	516.33	402.15	918.48	3.7769	99.55
80	18	820.96	449.87	1270.84	2.3754	62.61

HARNESS MASS & LOSS -- COPPER CONDUCTORS -- 400 c_m/amp

PVA volts	AWG	cond. mass gm	insul. mass gm	total mass gm	total resist ohm	power loss watts
28	16	1305.52	531.43	1836.95	1.4937	39.37
56	18	820.96	449.87	1270.84	2.3754	62.61
112	22	324.84	376.54	701.38	6.0033	158.23
80	20	516.33	402.15	918.48	3.7769	99.55

Table 5.5: PVA Bus Wiring Harness Mass and Loss - Copper

PVA BUS -- WIRE HARNESS MASS ESTIMATE

HARNESS MASS AND LOSS -- ALUMINUM CONDUCTORS -- 700 c_m/amp

PVA volts	AWG	cond. mass gm	insul. mass gm	total mass gm	total resist ohm	total loss watts
28	14	631.11	663.06	1294.17	1.5252	40.20
56	16	396.94	531.43	928.38	2.4250	63.92
112	20	156.99	402.15	559.14	6.1315	161.61
80	18	249.61	449.87	699.49	3.8563	101.64

HARNESS MASS & LOSS -- ALUMINUM CONDUCTORS -- 400 c_m/amp

PVA volts	AWG	cond. mass gm	insul. mass gm	total mass gm	total resist ohm	total loss watts
28	16	396.94	531.43	928.38	2.4250	63.92
56	18	249.61	449.87	699.49	3.8563	101.64
112	22	98.77	376.54	475.31	9.7459	256.87
80	20	156.99	402.15	559.14	6.1315	161.61

Table 5.6: PVA Bus Wiring Harness Mass - Aluminium

PVA BUS -- WIRE HARNESS MASS AND ELECTRICAL LOSS ESTIMATE

WIRE RUNS -- From each panel center to PMAD

Panel#	ctr to boom	boom to CL	CL to base	base to PMAD	total
Y+1	65.00	288.10	74.00	20.70	447.80 cm
Y+2	65.00	288.10	74.00	20.70	447.80 cm
Y+3	65.00	223.40	74.00	20.70	383.10 cm
Y+4	65.00	223.40	74.00	20.70	383.10 cm
Y+5	65.00	158.60	74.00	20.70	318.30 cm
Y+6	65.00	158.60	74.00	20.70	318.30 cm
Y+7	65.00	93.80	74.00	20.70	253.50 cm
Y+8	65.00	93.80	74.00	20.70	253.50 cm
Y-1	65.00	288.10	74.00	20.70	447.80 cm
Y-2	65.00	288.10	74.00	20.70	447.80 cm
Y-3	65.00	223.40	74.00	20.70	383.10 cm
Y-4	65.00	223.40	74.00	20.70	383.10 cm
Y-5	65.00	158.60	74.00	20.70	318.30 cm
Y-6	65.00	158.60	74.00	20.70	318.30 cm
Y-7	65.00	93.80	74.00	20.70	253.50 cm
Y-8	65.00	93.80	74.00	20.70	253.50 cm
array	1040.00	3055.60	1184.00	331.20	5610.80 cm

pwr/rtn run 11221.6 cm
112.216 m

Table 5.7: PVA Bus Wire Runs

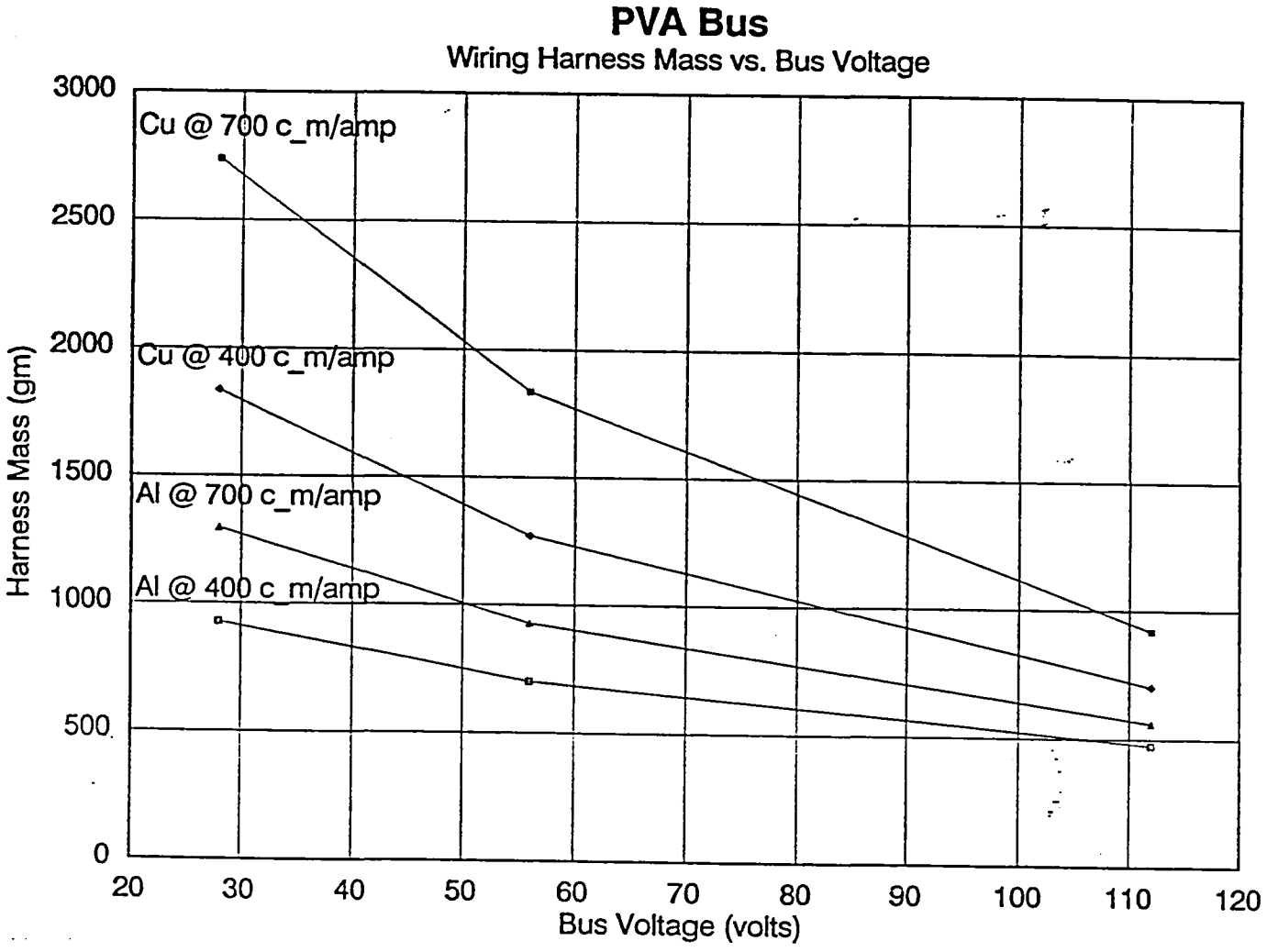

Figure 5.1: PVA Bus Harness Mass vs. Bus Voltage

5.2 Load Harness

The wiring harness conducting electrical power from the power distribution unit to the loads is considered next. Similarly, it is assumed that each load has a separate pair of insulated conductors, one for supply current and the other for return current. Mass and electrical losses at an operating voltage of 28 volts are determined. Results for conductors of copper and aluminum are presented for a current density of 700 circular mils per amp. These computations were performed using a 123R3 spreadsheet.

Table 5.8 lists the relevant parameters used to estimate harness weight and losses, as well as the wire properties at the selected voltages. Wire is assumed to be MIL-W-22759/16 with Tefzel insulation. The termination factor provides contingency for additional wire needed to route individual conductors to specific terminal locations, and accounts for wiring terminal weights. Wire gauges were selected from even gauges ranging from 0 AWG to 22 AWG. Selection results appear in Table 5.9.

Finer gauge wires were not considered since no appreciable weight savings could be obtained. This is largely because insulation accounts for over half of the weight of a 22 AWG wire. In addition, finer gauge wires tend to be fragile and are difficult to terminate and strain relieve.

Tables 5.10, and 5.11, present the mass estimate results and electrical resistance and loss estimates in tabular form, for the cable runs in Table 5.12 .

The wiring harness run lengths were estimated from spacecraft blueprints. Each current supply/return pair is assumed to run from the center of the PDU to a central point in the load cluster. Details of the run length associated with each panel appears in Table 5.12.

PARAMETERS

bus voltage 28.0 volts

	Watts	Amps
Mech	30.0	1.071
Therm	1.0	0.036
Cmd	10.0	0.357
Comm	36.0	1.286
GNC	37.9	1.354
Sci	222.0	7.929
total	336.9	12.032

	rho gm/cm^3	resist uohm-cm
Cu	8.890	1.742
Al	2.703	2.828

Term. factor	0.9
5.1E-06 cm^2/c_m	
c_m/amp	700

Table 5.8: Load Bus Wiring Harness Parameters

GAUGE SELECTION

	load amps	c_m/amp	min. c_m	Select	AWG	c_m
Mech	1.071	700	750		20	1021
Therm	0.036	700	25		22	643
Cmd	0.357	700	250		22	643
Comm	1.286	700	900		20	1021
GNC	1.354	700	948		20	1021
Sci	7.929	700	5550		12	6530

WIRE PROPERTIES

	AWG		Insul. gm/cm	Cond. gm/cm	Total gm/cm	Resist ohm/cm
Mech	20	Cu	0.04328	0.04601	0.08929	3.37E-04
Therm	22		0.03356	0.02895	0.06250	5.35E-04
Cmd	22		0.03356	0.02895	0.06250	5.35E-04
Comm	20		0.04328	0.04601	0.08929	3.37E-04
GNC	20		0.04328	0.04601	0.08929	3.37E-04
Sci	12		0.07788	0.29416	0.37204	5.26E-05
Mech	20	Al	0.04328	0.01399	0.05727	5.46E-04
Therm	22		0.03356	0.00880	0.04236	8.68E-04
Cmd	22		0.03356	0.00880	0.04236	8.68E-04
Comm	20		0.04328	0.01399	0.05727	5.46E-04
GNC	20		0.04328	0.01399	0.05727	5.46E-04
Sci	12		0.07788	0.08944	0.16732	8.55E-05

Table 5.9: Load Bus - Gauge Selection and Wire Properties

LOAD BUS -- WIRE HARNESS MASS ESTIMATE

HARNESS MASS & LOSS -- COPPER CONDUCTORS -- 700 c_m/amp

	insul. mass gm	cond. mass gm	term. mass gm	total mass gm	total resist ohm	power loss watts	eff
Mech	15.73	16.72	29.20	61.65	0.1223	0.140	0.995
Therm	12.19	10.52	20.44	43.16	0.1944	0.000	1.000
Cmd	12.19	10.52	20.44	43.16	0.1944	0.025	0.998
Comm	15.73	16.72	29.20	61.65	0.1223	0.202	0.994
GNC	15.73	16.72	29.20	61.65	0.1223	0.224	0.994
Sci	28.30	106.90	121.68	256.88	0.0191	1.203	0.995
total				528.14		1.794	

Table 5.10: Load Bus Wiring Harness Mass - Copper

LOAD BUS -- WIRE HARNESS MASS ESTIMATE

HARNESS MASS AND LOSS -- ALUMINUM CONDUCTORS -- 700 c_m/amp

	insul. mass gm	cond. mass gm	term. mass gm	total mass gm	total resist ohm	power loss watts	eff
Mech	15.73	5.08	18.73	39.54	0.1986	0.228	0.992
Therm	12.19	3.20	13.85	29.25	0.3156	0.000	1.000
Cmd	12.19	3.20	13.85	29.25	0.3156	0.040	0.996
Comm	15.73	5.08	18.73	39.54	0.1986	0.328	0.991
GNC	15.73	5.08	18.73	39.54	0.1986	0.364	0.990
Sci	28.30	32.50	54.72	115.53	0.0311	1.952	0.991
total				292.64		2.913	

Table 5.11: Load Bus Wiring Harness Mass - Aluminium

LOAD BUS -- WIRE HARNESS MASS ESTIMATE

WIRE RUNS -- from Power Distribution Unit

To:					total	pwr/rtn run
Mech	16.7	17.0	83.0	65.0	181.7	363.4 cm
Therm	16.7	17.0	83.0	65.0	181.7	363.4 cm
Cmd	16.0	0.0	0.0	0.0	16.0	32.0 cm
Comm	17.0	24.0	25.0	17.0	83.0	166.0 cm
GNC	43.0	35.0	25.0	17.0	120.0	240.0 cm
Sci	16.7	17.0	83.0	65.0	47.0	94.0 cm

Table 5.12: Load Bus Wiring Harness Runs

Appendix A

Peak Power FORTRAN Code

A fortran code was developed to determine the maximum power point for typical photovoltaic arrays at a range of temperatures. This code was used to develop the data presented in Figures 3.5 and 3.6.

```
      program Peak_Power

c     solves for a solar cell peak power voltage and current

      implicit none

      real*4  A       ! diode constant
      real*4  T, T_C  ! temperature (K) and (C)
      real*4  Vth     ! Vth = A k T / q
      real*4  Voc_25  ! O/C voltage @25C
      real*4  Voc     ! O/C voltage @T
      real*4  dVoc    ! O/C voltage temp sensitivity
      real*4  Jsc_25  ! S/C current density @25C
      real*4  Jsc     ! S/C current density @T
      real*4  dJsc    ! S/C current density temp sens
      real*4  FF_25   ! fill factor @25C
      real*4  FF      ! fill factor @T
      real*4  dFF     ! fill factor temp sensitivity

      real*4  Vmp     ! peak power voltage
      real*4  Jmp     ! peak power current density
```

```
      real*4  Pmp      ! peak power
      real*4  FFc      ! corrected form factor

      real*4  Voc_over_Vth
      real*4  Vmp_over_Voc

      real*4  k                ! boltzmans constant
      real*4  q                ! electron charge (coulomb)

      integer iter
      integer i

      k   = 1.38026E-23        ! joules/K
      q   = 1.6008E-19         ! coulomb

c     read diode parameters @ 25C (298.15K)

      open( unit=54, file='Pmp.inp')

      read( 54, *) A           ! diode constant
      read( 54, *) Voc_25      ! open circuit voltage
      read( 54, *) dVoc        ! V/K
      read( 54, *) Jsc_25      ! mA/cm^2
      read( 54, *) dJsc        ! mA/cm^2/K
      read( 54, *) FF_25       ! fill factor
      read( 54, *) dFF         ! fill factor sensitivity

      open( unit=55, file='Pmp.prn')
      write( 55, 109) A
109   format(1x, g13.5, '    "A - diode constant"')
      write( 55, 108) Voc_25
108   format(1x, g13.5, '    "Voc @ 25C"')
      write( 55, 107) dVoc
107   format(1x, g13.5, '    "dVoc/dT (V/K)"')
      write( 55, 106) Jsc_25
106   format(1x, g13.5, '    "Jsc @ 25C"')
      write( 55, 105) dJsc
105   format(1x, g13.5, '    "dJsc/dT (mA/cm^2/K)"')
      write( 55, 104) FF_25
```

```
104     format(1x, g13.5, '    "FF @ 25C"')
        write( 55, 103) dFF
103     format(1x, g13.5, '    "dFF/dT"'/)

        write( 55, 102)
102     format(' "T(K)"', 2x,
     .    '"Vmp"', 8x, '"Jmp"', 8x, '"Pmp"', 8x, '"FFc"', 8x,
     .    '"Vth"', 8x, '"Voc"', 8x, '"Jsc"', 8x, '"FF "', 5x,
     .    '"iter"')

        do i = 173, 423

        T = i
        Vth = A * k * T / q
        T_C = T - 273.15

c       correct Voc, Jsc and FF for temperature

        Voc = Voc_25 + (dVoc * ( T - 298.15))
        Jsc = Jsc_25 + (dJsc * ( T - 298.15))
        FF  = FF_25  + (dFF  * ( T - 298.15))
        Vmp = sqrt( FF) * Voc   ! initial guess

        call find_Vmp( Voc, Vth,
     .      Vmp, Voc_over_Vth, Vmp_over_Voc, iter)

        call find_Jmp( Vth, Voc, Vmp, Jsc,
     .                 Jmp, Pmp, FFc)

        write( *, 111) T, T_C, Vth
111     format(/' T(K) =', g13.6, ' T(C) =', g13.5,
     .          ' Vth  =', g13.6)
        write( *, 112) Voc, Jsc, FF
112     format( ' Voc  =', g13.6, ' Jsc  =', g13.5,
     .          ' FF   =', g13.6)
        write( *, 113) Vmp, iter
113     format( ' Vmp          =', g13.6,
     .          ' iter =', i5)
        write( *, 114) Voc_over_Vth, Vmp_over_Voc
```

```
114     format( ' Voc_over_Vth =', g13.6,
     .          ' Vmp_over_Voc =', g13.6)
        write( *, 115) Jmp, FFc
115     format( ' Jmp          =', g13.6,
     .          ' FFc          =', g13.6)

        write( 55, 101) T, Vmp, Jmp, Pmp, FFc,
     .                  Vth, Voc, Jsc, FF, iter
101     format( 1x, f4.0, 8g13.6, i5)

        enddo

        close( unit=55)
        stop
        end



        subroutine find_Vmp( Voc, Vth,
     .             Vmp, Voc_over_Vth, Vmp_over_Voc, iter)

c       solves for the peak power voltage for a solar cell

        implicit none

        real*4  Voc             ! open circuit voltage @T
        real*4  Vth             ! Vth = A k T / q
        real*4  alpha           ! alpha = 1/Vth

        real*4  Vmp             ! current estimate
        real*4  Vp              ! previous estimate
        real*4  Vmp0            ! initial estimate
        real*4  F, F_prime
        real*4  delta
        integer iter
        real*4  Voc_over_Vth, Vmp_over_Voc
```

```
        Vmp0 = Vmp      ! initial guess
        Vp   = Vmp
        alpha = 1/Vth

        do iter = 1, 1000

        Vmp = Vp - F( Vp, Voc, alpha)/ F_prime( Vp, Voc, alpha)
        delta = abs((Vmp - Vp) / Vp)
c       write( *, 101) iter, Vmp, Vp, delta
c101    format( i4, '  Vmp =', g13.6, '  Vp =', g13.6,
c     .          ' delta =', g13.6)

        if( delta .lt. 1.0E-6) then
           Voc_over_Vth = Voc / Vth
           Vmp_over_Voc = Vmp / Voc
           return
        else
           Vp = Vmp
        endif

        enddo

        write( *, *) 'Convergence Failure'
c       write( *, 101) iter, Vmp, Vp, delta

        return
        end




        function F( V, Voc, alpha)

        implicit none
        real*4  F
        real*4  V
        real*4  Voc
        real*4  alpha
```

```
      F = 1 + alpha*V - exp( alpha*( Voc - V))
c     write( *, 102) F, V, Voc, alpha
c102  format( ' F     =', g13.6, ' V =', g13.6,
c    .        ' Voc =', g13.6, ' alpha =', g13.6)
      return
      end



      function F_prime( V, Voc, alpha)

      implicit none
      real*4  F_prime
      real*4  V
      real*4  Voc
      real*4  alpha

      F_prime = alpha + alpha*exp( alpha*( Voc - V))
c     write( *, 103) F_prime, V, Voc, alpha
c103  format( ' Fprime=', g13.6, ' V =', g13.6,
c    .        ' Voc =', g13.6, ' alpha =', g13.6)
      return
      end



      subroutine find_Jmp( Vth, Voc, Vmp, Jsc,
     .                     Jmp, Pmp, FFc)

c     solves for the peak power current for a solar cell

      implicit none

      real*4  Vth     ! Vth = A k T / q
      real*4  Voc     ! O/C voltage @T
      real*4  Jsc     ! S/C current density @T
      real*4  Vmp     ! peak power voltage
      real*4  Jmp     ! peak power current density
```

```
real*4  Pmp      ! peak power
real*4  FFc      ! corrected form factor

Jmp = Jsc*(exp(Voc/Vth)-exp(Vmp/Vth))/(exp(Voc/Vth)-1)
Pmp = Vmp * Jmp
FFc = Pmp / (Voc*Jsc)
return
end
```

REPORT DOCUMENTATION PAGE

Form Approved
OMB No. 0704-0188

Public reporting burden for this collection of information is estimated to average 1 hour per response, including the time for reviewing instructions, searching existing data sources, gathering and maintaining the data needed, and completing and reviewing the collection of information. Send comments regarding this burden estimate or any other aspect of this collection of information, including suggestions for reducing this burden, to Washington Headquarters Services, Directorate for Information Operations and Reports, 1215 Jefferson Davis Highway, Suite 1204, Arlington, VA 22202-4302, and to the Office of Management and Budget, Paperwork Reduction Project (0704-0188), Washington, DC 20503.

1. AGENCY USE ONLY (*Leave blank*)	2. REPORT DATE	3. REPORT TYPE AND DATES COVERED
	September 1995	Technical Memorandum

4. TITLE AND SUBTITLE

TROPIX Power System Architecture

5. FUNDING NUMBERS

WU-233-03-05

6. AUTHOR(S)

David B. Manner and J. Mark Hickman

7. PERFORMING ORGANIZATION NAME(S) AND ADDRESS(ES)

National Aeronautics and Space Administration
Lewis Research Center
Cleveland, Ohio 44135-3191

8. PERFORMING ORGANIZATION REPORT NUMBER

E-8975

9. SPONSORING/MONITORING AGENCY NAME(S) AND ADDRESS(ES)

National Aeronautics and Space Administration
Washington, D.C. 20546-0001

10. SPONSORING/MONITORING AGENCY REPORT NUMBER

NASA TM-106660

11. SUPPLEMENTARY NOTES

David B. Manner, Sverdrup Technology, Inc., Ames Research Center, Moffett Field, California and J. Mark Hickman, NASA Lewis Research Center. Responsible person, J. Mark Hickman, organization code 6850, (216) 977-7105.

12a. DISTRIBUTION/AVAILABILITY STATEMENT

Unclassified - Unlimited
Subject Category 20

This publication is available from the NASA Center for Aerospace Information, (301) 621-0390.

12b. DISTRIBUTION CODE

13. ABSTRACT (*Maximum 200 words*)

This document contains results obtained in the process of performing a power system definition study of the TROPIX power management and distribution system (PMAD). Requirements derived from the PMADs interaction with other spacecraft systems are discussed first. Since the design is dependent on the performance of the photovoltaics, there is a comprehensive discussion of the appropriate models for cells and arrays. A trade study of the array operating voltage and its effect on array bus mass is also presented. A system architecture is developed which makes use of a combination of high efficiency switching power convertors and analog regulators. Mass and volume estimates are presented for all subsystems.

14. SUBJECT TERMS

Solar electric propulsion; Power system; Power management and distribution (PMAD)

15. NUMBER OF PAGES

76

16. PRICE CODE

A05

17. SECURITY CLASSIFICATION OF REPORT	18. SECURITY CLASSIFICATION OF THIS PAGE	19. SECURITY CLASSIFICATION OF ABSTRACT	20. LIMITATION OF ABSTRACT
Unclassified	Unclassified	Unclassified	

National Aeronautics and
Space Administration

Lewis Research Center
21000 Brookpark Rd.
Cleveland, OH 44135-3191

Official Business
Penalty for Private Use $300

POSTMASTER: If Undeliverable — Do Not Return